# USC–SIPI REPORT #243

**Analysis of Real Sonar Signals Using Non-Linear Signal Processing**

**by**

**Sam Heidari and Chrysostomos L. Nikias**

**September 1993**

Signal and Image Processing Institute
**UNIVERSITY OF SOUTHERN CALIFORNIA**
Department of Electrical Engineering-Systems
3740 McClintock Avenue, Room 404
Los Angeles, CA 90089-2564 U.S.A.

# Analysis of Real Sonar Signals Using Non-linear Signal Processing†

**Sam Heidari and Chrysostomos L. Nikias**
Signal and Image Processing Institute, University of Southern California,
Los Angeles, CA 90089-2564

## 1.0 Abstract

Various sequential real sonar data files are analyzed through different signal processing algorithms. Data files are divided into two groups: files consisting of a signal of interest (SOI) with additive noise and files consisting of pure noise. The purpose of these analyses is to determine if a given data record contains the SOI. Methods of Power Spectrum Density estimation, Higher-order Spectrum estimation and Local Intrinsic Dimension (LID) estimation are applied. A new method is introduced in LID estimation using higher-order off diagonal cumulants and shown to be more consistent in categorizing the SOIs. Further work needs to be done using Higher-order spectra-based time-frequency techniques for non-stationary analysis due to the time-varying nature of the signals.

## 2.0 Introduction

Six sequential real sonar data files (TP1, TP13, TP15, TP2, TP25, and TP6) have been analyzed through various signal processing methods. Data files TP13, TP15, TP2, and TP6 consist of a signal of interest component with additive noise, where data files TP1 and TP25 consist of pure noise processes. The nature of noise is unknown. The purpose of this work is to analyze the data and to present discrimination methods to identify the signal plus noise data from the noise only data. Various methods were applied for this purpose. The applied methods may be separated into three major groups: Power spectrum methods, Higher-order spectrum methods, and local intrinsic dimension (LID) estimation methods. Here, the Welch method and Yule-Walker method were used for power spectrum analysis. The higher-order spectrum analysis consists of applying the bispectrum and Third-Order Recursion (TOR) Methods. Covariance LID (CLID) [6], higher-order diagonal LID (HOLID-D) [7], and a new method using higher-order off diagonal LID (HOLID-OD) were applied under the LID category. A description of these methods is given in sections 3-5. In section 6, we present the test results of HOLID-OD for Lorenz and Henon Maps. Section 7 demonstrates the results of applying these algorithms to the real sonar data files.

†This work was supported under the Office of Naval Research Contract No. N00014-91-J-4021

# 3.0 Power Spectrum Methods

Power Spectral Density (PSD) by definition is the distribution of power among the frequency components of the signal under consideration. This is equivalent to the discrete time Fourier transform of the autocorrelation sequence. Since our data is finite and it contains noise, an estimate of the PSD is achieved through using Welch and Yule-Walker methods.

## 3.1 Welch Method

The Welch method is one of the classical power spectrum estimation methods [1]. It is implemented as follows:

- Segment the data into non-overlapping M records of L samples each. $\{x^{(i)}(n)\}$ for $n=0,...,$L-1 and $i=1,...,M$
- Using a Hanning window, estimate periodogram of each segment

$$J_L^{(i)}(k) = \frac{1}{LU}\left|\sum_{n=0}^{L-1} x^{(i)}(n)\, w(n)\, e^{-j\frac{2\pi}{L}nk}\right|^2 \qquad \text{for i=1,2,...,M}$$

$$U = \frac{1}{L}\sum_{n=0}^{L-1} |w(n)|^2$$

- Average periodogram

$$S(k) = \frac{1}{M}\sum_{i=1}^{M} J_L^{(i)}(k) \qquad \text{for } k=0,...,(L/2)-1$$

- $S(k)$ is the Welch periodogram of the signal.

## 3.2 Yule-Walker Method

The Yule-Walker (YW) method is based on the assumption that the data is generated from an autoregressive (AR) system [2]. In order to estimate the PSD, coefficients of the AR model are calculated from the estimate of the autocorrelation lags of the data. The power spectrum density will be defined from these system coefficients. The following steps demonstrate the implementation of YW method:

- Estimate biased autocorrelation lags

$$\hat{R}(\tau) = \frac{1}{N}\sum_{n=1}^{N-|\tau|} x(n)\, x(n+\tau) \qquad \text{for } \tau=0,...,M$$

- Form the YW equations or "normal equations"

$$\begin{bmatrix} \hat{R}(0) & \hat{R}(1) & \dots & \hat{R}(M) \\ \hat{R}(1) & \hat{R}(0) & \dots & \hat{R}(M-1) \\ \dots & \dots & \dots & \dots \\ \hat{R}(M) & \hat{R}(M-1) & \dots & \hat{R}(0) \end{bmatrix} \begin{bmatrix} 1 \\ a_{M,1} \\ a_{M,2} \\ \dots \\ a_{M,M} \end{bmatrix} = \begin{bmatrix} Q_M \\ 0 \\ \dots \\ 0 \end{bmatrix}$$

- Use the Levinson-Durbin algorithm to solve for $\{a_{M,1},\dots,a_{M,M}\}$ and $Q_M$
- PSD is defined as:

$$S(\omega) = \frac{Q_M}{\left|1 + \sum_{i=1}^{M} a_{M,i} e^{-j\omega Ti}\right|^2} \qquad \text{for } |\omega| \le \pi$$

# 4.0 Higher-Order spectra

The following properties of higher-order spectra (polyspectra) [3 and 4] make them very attractive for use in signal processing: (1) suppress the additive Gaussian noise and in the case of bispectrum this is also true for non-Gaussian noise processes with symmetric probability density function (pdf); (2) detect and characterize the nonlinearities in the data; and (3) preserve the phase information of the system. Here, the conventional Bispectrum and parametric TOR methods are the Higher-order spectrum methods used [3].

## 4.1 Bispectrum

The conventional method of determining the bispectrum is used here,

- Data is segmented in $M$ parts of length L each

$$\{x^{(i)}(n)\} \qquad i=1,\dots,M \text{ and } n=0,\dots,L-1$$

- Fourier transform of each segment is calculated,

$$X^{(i)}(\omega) = FFT\{x^{(i)}\}$$

- Bispectrum for each segment is:

$$B^{(i)}(\omega_1,\omega_2) = X^{(i)}(\omega_1)X^{(i)}(\omega_2)X^{(i)*}(\omega_1+\omega_2)$$

$$\text{for } |\omega_1 + \omega_2| \le 1 \text{ (assume T =1)}$$

- Average bispectrum is calculated as:

$$B(\omega_1 + \omega_2) = \frac{1}{M} \sum_{i=1}^{M} B^{(i)}(\omega_1 + \omega_2)$$

## 4.2 TOR Method

This method was introduced by Raghuveer and Nikias [3]. The TOR method is a parametric technique based on autoregressive (AR) modeling of the third order cumulants. The following steps describe the implementation of TOR.

- Form the biased third moment estimates as follows:

  - ❑ Segment the data into $K$ records of $M$ samples each

  - ❑
$$r^{(i)}(m,n) = \frac{1}{M} \sum_{l=\min(1,1-n,1-m)}^{\min(M,M-n,M-m)} X_l^{(i)} X_{l+m}^{(i)} X_{l+n}^{(i)} \qquad \text{for i=1,...,K}$$

  - ❑
$$\hat{R}(m,n) = \frac{1}{K} \sum_{i=1}^{K} r^{(i)}(m,n)$$

- Form the system of linear equations:

$$\begin{bmatrix} \hat{R}(0,0) & \hat{R}(1,1) & \dots & \hat{R}(p,p) \\ \hat{R}(1,1) & \hat{R}(0,0) & \dots & \hat{R}(p-1,p-1) \\ \dots & \dots & \dots & \dots \\ \hat{R}(-p,-p) & \hat{R}(-p+1,-p+1) & \dots & \hat{R}(0,0) \end{bmatrix} \begin{bmatrix} 1 \\ a_1 \\ a_2 \\ \dots \\ a_p \end{bmatrix} = \begin{bmatrix} \hat{\beta} \\ 0 \\ \dots \\ 0 \end{bmatrix}$$

- Solve for $\{a_i\}$, i=1,...,p.
- The bispectrum estimate is

$$B(\omega_1,\omega_2) = H(\omega_1)H(\omega_2)H^*(\omega_1+\omega_2)$$

$$\text{where } H(\omega) = \frac{1}{1 + \sum_{n=1}^{p} a_n exp(-j\omega n)} \qquad \text{for } |\omega| \le \pi$$

We present the value of $H(\omega)$ in section 6.

# 5.0 LID Analysis

Passamante, Hediger and Gollub in [6], Passamante and Farrell in [7], and Broomhead, Jones and King in [8] suggested different methods of estimating the fractal dimension

(FD) for chaotic signals using the local intrinsic dimension (LID). In [6] and [8] respectively, the covariance (CLID) and higher-order diagonal (HOLID-D) information contained in the local data points in the embedded space were analyzed. CLID and HOLID-D methods demonstrate more robustness to the presence of additive noise than the traditional FD estimation algorithms such as Grassberger and Procaccia algorithm (GPA) [5], but still are very sensitive to the choice of embedding dimension r for fixed delay (or the window size). Here, we introduce a new LID estimation method which is less sensitive to noise and the embedding dimension r. This technique is based on the fourth order off diagonal cumulant matrix of the chaotic signal. This new technique will be referred as HOLID-OD.

## 5.1 Description of CLID, HOLID-D, and HOLID-OD methods

Assume the chaotic system generating the signal consists of $n$ differential equations in $n$ variables. These set of equations may be transformed into an $n^{th}$-order equation of just one variable via successive differentiations and eliminations. Therefore, everything is known about the system of equations, if one variable is known at all times. Lets say, we are able to observe only the discrete data of one variable, $\{x_i\}$ for $i=1,2,...,N$ (which is very typical). Here, $\{x_i\}$ consists of a deterministic signal of interest, $s_i$, and additive mean-zero, white Gaussian noise, $w_i$,

$$x_i = s_i + w_i \qquad \text{(EQ 1)}$$

Theorems of Takens [12] and Mane [15] state for infinitely long noiseless sequential data $\{x_i\}$ and any non-zero time delay $\tau$, an attractor may be constructed in an r-dimensional space, which will be diffeomorphicaly equivalent to the attractor in the phase space. This attractor is formed through embedding the sequential data $\{x_i\}$ in $r$-dimensional space as follows:

$$\mathbf{x}_1=[x_1,x_{1+\tau},...,x_{1+(r-1)\tau}]$$

$$\mathbf{x}_2=[x_2,x_{2+\tau},...,x_{2+(r-1)\tau}]$$

...

$$\mathbf{x}_n=[x_n,x_{n+\tau},...,x_{n+(r-1)\tau}] \qquad \text{(EQ 2)}$$

where vectors $\mathbf{x}_1, \mathbf{x}_2,...,\mathbf{x}_n$ represent the attractor in the embedding space. For the theorem to hold, it is required that $r \geq 2d+1$, where $d$ is the topological dimension of the attractor, and it is usually unknown. Theoretically the choice of $\tau$ is not important for noiseless data of infinite length. In practical cases [15], the FD estimation is sensitive to the choice of the window size $T=(r-1)\tau$. This sensitivity is not individual to the choice of embedding dimension r, or delay $\tau$, but to the window size T.

Once the attractor is formed, for all the LID based methods, we start by choosing $L$ arbitrary data samples on the attractor to serve as local centers, $c_i$, for $i=1,...,L$. Next, we will determine $q$ nearest data vectors to these local centers in the embedded space. We refer to q neighbors of $c_i$ as $x_{i1},x_{i2},...,x_{iq}$, where $x_{i1}$ is the closest vector to the local center $c_i$ in the embedded space and $x_{iq}$ is the $q^{th}$ farthest vector. Note that $q$ is a fixed number that should

be large enough to reduce the effect of the noise, but small enough for the subspace consisting of the $q$ neighbor vectors to be linear. At the local center $c_i$, define vectors $y_{ij}=x_{ij}-c_i$ for $j=1,...q$. To calculate the CLID, $y_{ij}$ vectors are used to form $(r \times q)$ matrix $X_i$. All the LID methods introduced here only differ in the way $X_i$ is created. For CLID method, $X_i$ is formed [6 and 8] at all the local centers as follows:

$$X_i=[y_{i1},y_{i2},...,y_{iq}] \qquad \text{(EQ 3)}$$

LID of the data at the local center $i$ is calculated by applying Singular Value Decomposition (SVD) on the $X_i$. The singular values are the square roots of the eigenvalues of the auto-covariance of the local data. For the noise free case, the rank of the matrix corresponds to the degree of local nonlinearity. In our case, the eigenvalues of $X_i$ form two distinct groups: eigenvalues belonging to SOI and eigenvalues of additive noise. CLID is defined as the number of eigenvalues corresponding to SOI. A threshold value must be set to separate two groups of eigenvalues. Since the values of CLID is different at each local center the average of CLID, <CLID>, is calculated at all the local centers. <CLID> is a measure of second-order dimensionality of the attractor.

In HOLID-D and HOLID-OD methods the fourth-order cumulant function is used to estimate $X_i$. Passamante *et al* introduced[7] HOLID-D using fourth-order symmetric cumulant slice, $c_4(0,0,\tau)$. For HOLID-OD, we use two off-diagonal cumulant slices $c_4(0,\tau,2\tau)$ and $c_4(0,\tau,3\tau)$.

Fourth-order cumulants of zero-mean real random variables is defined as [7]:

$$\begin{aligned} c_4(\tau_1,\tau_2,\tau_3) &= E\{x(t),x(t+\tau_1),x(t+\tau_2),x(t+\tau_3)\} \\ &-E\{x(t)x(t+\tau_1)\}E\{x(t+\tau_2)x(t+\tau_3)\} \\ &-E\{x(t)x(t+\tau_2)\}E\{x(t+\tau_1)x(t+\tau_3)\} \\ &-E\{x(t)x(t+\tau_3)\}E\{x(t+\tau_1)x(t+\tau_2)\} \end{aligned} \qquad \text{(EQ 4)}$$

In HOLID-D approach, the matrix $X_i$ is created using $c_4(0,0,\tau)$ slice as follows:

$$X_i = C_4\left(\begin{bmatrix} y_1^3 \\ y_2^3 \\ \cdots \\ y_r^3 \end{bmatrix}\begin{bmatrix} y_1 & y_2 & \cdots & y_r \end{bmatrix}\right) \qquad \text{(EQ 5)}$$

where $y_i$ is the $i^{th}$ element of a neighborhood vector with the local center subtracted from it. The statistical expectation values are calculated by averaging the $q$ local data points of each local center. Using (EQ 1), each element of $X_i$ is estimated as:

$$X_{ij} = E\{y_i^3 y_j\} - 3E\{y_i^2\}E\{y_i y_j\} \qquad \text{(EQ 6)}$$

Similar to CLID method, the number of significant eigenvalues of $X_i$ correspond to HOLID-D. The average HOLID-D, <HOLID-D>, is found for all the local centers.

In HOLID-OD algorithm, $X_i$ is an off diagonal (non- symmetric) fourth-order cumulant matrix, where $c_4(0,\tau,2\tau)$ and $c_4(0,\tau,3\tau)$ slices are used instead of $c_4(0,0,\tau)$. For $c_4(0,\tau,2\tau)$ and $c_4(0,\tau,3\tau)$ slices matrices $X_{i1}$ ($\frac{r}{3}\times\frac{r}{3}$) and $X_{i2}$ ($\frac{r}{4}\times\frac{r}{4}$) are presented respectively as follows:

$$X_{i1} = c_4\left(\begin{bmatrix} y_1^2y_2y_3 & y_1^2y_3y_5 & \cdots & y_1^2y_{\frac{r}{3}+1}y_{\frac{2r}{3}+1} \\ y_2^2y_3y_4 & y_2^2y_4y_6 & \cdots & y_2^2y_{\frac{r}{3}+2}y_{\frac{2r}{3}+2} \\ \cdots & \cdots & \cdots & \cdots \\ y_{\frac{r}{3}}^2y_{\frac{r}{3}+1}y_{\frac{r}{3}+2} & y_{\frac{r}{3}}^2y_{\frac{r}{3}+2}y_{\frac{r}{3}+4} & \cdots & y_{\frac{r}{3}}^2y_{\frac{2r}{3}}y_r \end{bmatrix}\right) \quad \text{(EQ 7)}$$

where $y_i$'s are same as $y_i$'s in HOLID-D. The $i,j$ element of the $X_{i1}$ matrix is defined as:

$$X_{i1}{}_{i,j} = C_4(y_i^2y_{i+j}y_{i+2j}) = E\{y_i^2y_{i+j}y_{i+2j}\} \quad \text{(EQ 8)}$$

$$-E\{y_i^2\}E\{y_{i+j}y_{i+2j}\} - 2E\{y_iy_{i+j}\}E\{y_iy_{i+2j}\}$$

Similarly $X_{i2}$ is defined as:

$$X_{i2} = c_4\left(\begin{bmatrix} x_1^2x_2x_4 & x_1^2x_3x_7 & \cdots & x_1^2x_{\frac{r}{4}+1}x_{\frac{3r}{4}+1} \\ x_2^2x_3x_5 & x_2^2x_4x_8 & \cdots & x_2^2x_{\frac{r}{4}+2}x_{\frac{3r}{4}+2} \\ \cdots & \cdots & \cdots & \cdots \\ x_{\frac{r}{4}}^2x_{\frac{r}{4}+1}x_{\frac{r}{4}+3} & x_{\frac{r}{4}}^2x_{\frac{r}{4}+2}x_{\frac{r}{4}+6} & \cdots & x_{\frac{r}{4}}^2x_{\frac{r}{2}}x_r \end{bmatrix}\right) \quad \text{(EQ 9)}$$

and its elements,

$$X_{i2}{}_{i,j} = C_4(x_i^2x_{i+j}x_{i+3j}) = E\{x_i^2x_{i+j}x_{i+3j}\} \quad \text{(EQ 10)}$$

$$-E\{x_i^2\}E\{x_{i+j}x_{i+3j}\} - 2E\{x_ix_{i+j}\}E\{x_ix_{i+3j}\}$$

Again, expectations are calculated by averaging the $q$ local data points of each of the local centers. Using SVD, the effective rank of the matrix $X_i$ are determined for each local center, which represents the HOLID-OD of the attractor at that position in the phase space. Average HOLID-OD, <HOLID-OD>, is calculated over all local centers.

## 6.0 Numerical Results for experimental data

To demonstrate the HOLID-OD approach, the results are tested for Lorenz and Henon systems and then applied to our real sonar data sequences. The simulation is done for CLID, HOLID-D and HOLID-OD methods and results are compared. The Henon data is generated by

$$x(n) = bx(n-2) + 1 - ax(n-1)^2$$

where $a$=1.4 and $b$=0.3. The initial conditions are $x(0)= x(-1)$=0.

The Lorenz equations are defined as:

$$\dot{x} = a(y-x)$$

$$\dot{y} = cx - y - xz$$

$$\dot{z} = -bz + xy$$

where $a$=10, $c$=28 and $b$=8/3. In generating the Lorenz data, the initial conditions are $x(0)=y(0)=z(0)$=1. The data was generated via Runge-Kutta integration with a step size equal to 0.003. For these results, the number of sample points, n, is 10,000 and the number of vectors in each neighborhood, $q$=40. The time delay is kept fixed throughout the simulations and the value of embedding dimension is varied.

Figures 6.1 and 6.2 illustrate that at thresholds of 15% and 30% of the largest eigenvalue, for the Henon map, HOLID-ODs are less sensitive to changes of the embedding dimension $r$. The solid straight line is the true fractal dimension of Henon map, which is equal to 1.21.

Figures 6.3 and 6.4 are similar to 6.1 and 6.2 for the Lorenz map. Here, we may observe that at the presence of noise, the performance of CLID deteriorates. This is not true for HOLID-OD. The solid straight line is the true fractal dimension of Lorenz map, which is 2.05.

Applying the methods to the real sonar data shows that HOLID-OD in their cases is also less sensitive to changes of the embedding dimension r (figs. 6.5 and 6.6).

# 7.0 Numerical results for real data

Figures 7.1-7.21 present the results for the real data analysis. Figure 7.1 is a window of the time representation of the signals. It shows that signals are very similar in the time domain. Figure 7.2 is the PSD of the signals estimated through the Welch method. Each data segment contains 2048 samples and about 5,000,000 to 6,000,000 samples were used for the implementation of this method. We also estimated PSD using Yule-Walker for AR model orders of 20,30,40, and 50 (figs. 7.3 - 7.6). As it is seen in fig. 7.7, AIC indicates a model order of 20 is sufficient for the Yule-Walker method implementation. Auto-correla-

tion was estimated from 5,000,000 to 6,000,000 samples. Next, the Welch and Yule-Walker methods were applied to 32768 data samples instead of the entire data to demonstrate that smaller segments of the data has the same characteristic as the entire data, (figs. 7.8-7.11). With this in mind, the rest of the analyses are done for the same smaller segment of the data files. None of PSD analyses are able to distinguish signal plus noise data files from pure noise files.

The TOR method was applied to the data files and the magnitude and phase estimation of $H(\omega)$ is presented in figs. 7.12-7.15 for order, p, equal to 20 and 50. In fig. 7.16 we present the singular values of cumulant matrix used for TOR estimation. Also, we were not able to categorize the data files using TOR.

The Bispectrum of data files $B(\omega_1,\omega_2)$ is presented in fig. 7.17. It is noticeable that there exists a difference between the signal plus noise cases and the noise only cases. This difference is especially visible when either $\omega_1$ or $\omega_2$ are fixed at a low frequency and the other is varied. Therefore, bispectrum may be used as a visual tool to distinguish given cases.

The next step of our analysis involves LID estimation. The results for CLID, HOLID-D and HOLID-ODs are presented in figs. 7.18 and 7.19. for embedding dimension, r, equal to 20, 30, 40, and 50 and for thresholds of 15% and 30% of the largest singular value. Setting the optimum threshold is an area of research on its own. Here, the threshold values are chosen arbitrarily. For r equal to 20, 40, or 50 and the threshold of 30%, the HOLID-OD, using $c_4(0,\tau,3\tau)$ cumulant slice, shows a higher value for the pure noise cases than the signal plus noise cases (fig 7.20). HOLID-OD methods are more consistent than other LID estimation methods to categorize the data files.

Next, data files are passed through a low passed filter (fig. 7.21 is the PSD of the low pass filtered the data files), and then LID estimation methods are applied. For r equals 30, CLID demonstrates higher values for noise only cases and the same is true for HOLID-OD, $c_4(0,\tau,3\tau)$ slice, at r equals 20 (fig. 7.20), otherwise most of the methods failed for the low pass filtered data.

# 8.0 Conclusion

While most of the applied methods failed to categorize the data files, careful examination of the results reveals that we are able to utilize the bispectrum of data as a visual discrimination tool. Also, the average HOLID-OD using the $C_4(0,\tau,3\tau)$ slice is able to distinguish between the noise only and the signal plus noise cases, for r = 20, 40, 50 and the threshold = 30% of the largest singular value. The introduced methods of HOLID-OD are less sensitive to the embedding dimension r and more robust in the presence of noise than the previously known LID methods. Let's note that the average LIDs are random variables and their statistical properties should be studied. One way to get more stable results is to decrease the variance of average LID by increasing the number of local centers. This would increase the computation. Because of the nature of the signal, further work needs to

be done using higher-order spectra-base time-frequency techniques for non-stationary signal analysis.

## 9.0 References


[1] S. L. Marple, *Digital Spectral Analysis with Applications,* Prentice-Hall, Englewood Cliffs, NJ, 1987, pp. 154-158.

[2] S. L. Marple, *Digital Spectral Analysis with Applications,* Prentice-Hall, Englewood Cliffs, NJ, 1987, pp. 172-188.

[3] C. L. Nikias and A. P. Petropulu, Higher - Order Spectral Analysis, Prentice Hall, Englewood Cliffs, NJ, 1993.

[4] C. L. Nikias and M. R. Raghuveer, "Bispectrum Estimation: A Digital Signal Processing Framework," Proceedings IEEE, 75(7), pp. 869-891, July 1987.

[5] P. Grassberger and I. Procaccia, Phys. Rev. Lett. 50, 346 (1983)

[6] A. Passamante, T. Hediger, and M. Gollub, Phys. Rev. A 39, 3640 (1989).

[7] A. Passamante and Mary Eileen Farrell, Phys. Rev. A 43, 5268 (1990).

[8] D. S. Broomhead, R. Jones, and G. P. King, J. Phys. A 20, L563 (1987)

[9] B. B. Mandelbrot, *The Fractal Geometry of Nature,* (Freeman, New York, 1982).

[10] T. Hediger, A. Passamante, and Mary Eileen Farrell, Phys. Rev. A 41, 5325 (1990).

[11] P. Flandrin and O. Michel, IEEE, Signal Processing Workshop on Higher-Order Statistics, 295, 1993.

[12] F. Takens, in *Dynamical Systems of Turbulence,* edited by D. A. Rand and L. S. Young (Springer, Berlin, 1981).

[13] N. H. Packard, J.P. Crutchfield, J. D. Farmer, and R. S. Shaw, Phys. Rev. Lett. 45, 712 (1980).

[14] T. S. Parker and L. O. Chua, Proc. of The IEEE, Vol. 75, No. 8, 982 (1987).

[15] A. M. Albano, J. Muench, C. Schwartz, A. I. Mees, and P. E. Rapp, Phys. Rev. A, Vol. 38, No. 6, Spet. 15, 3017 (1980).

## 10.0 Figures

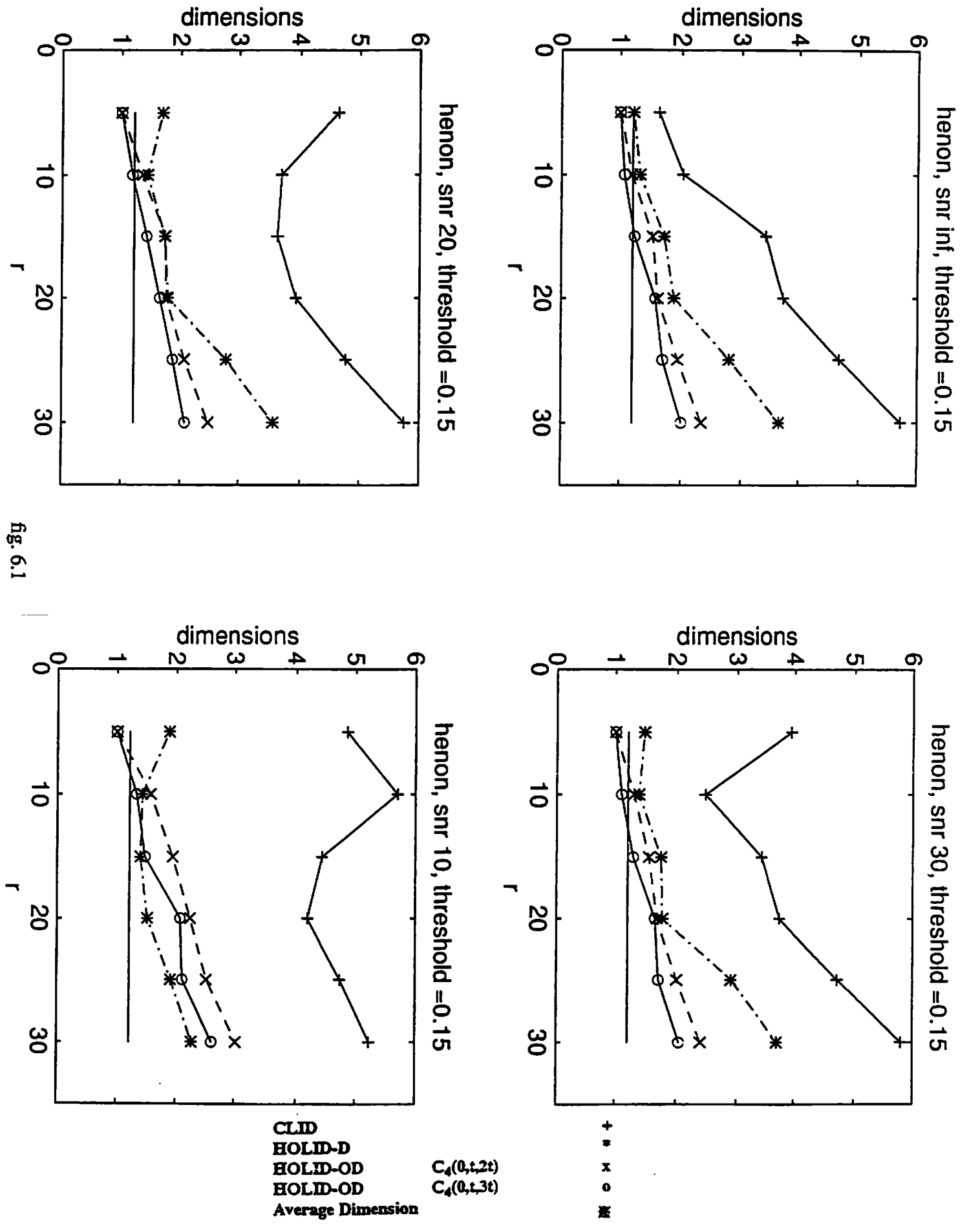


fig. 6.1

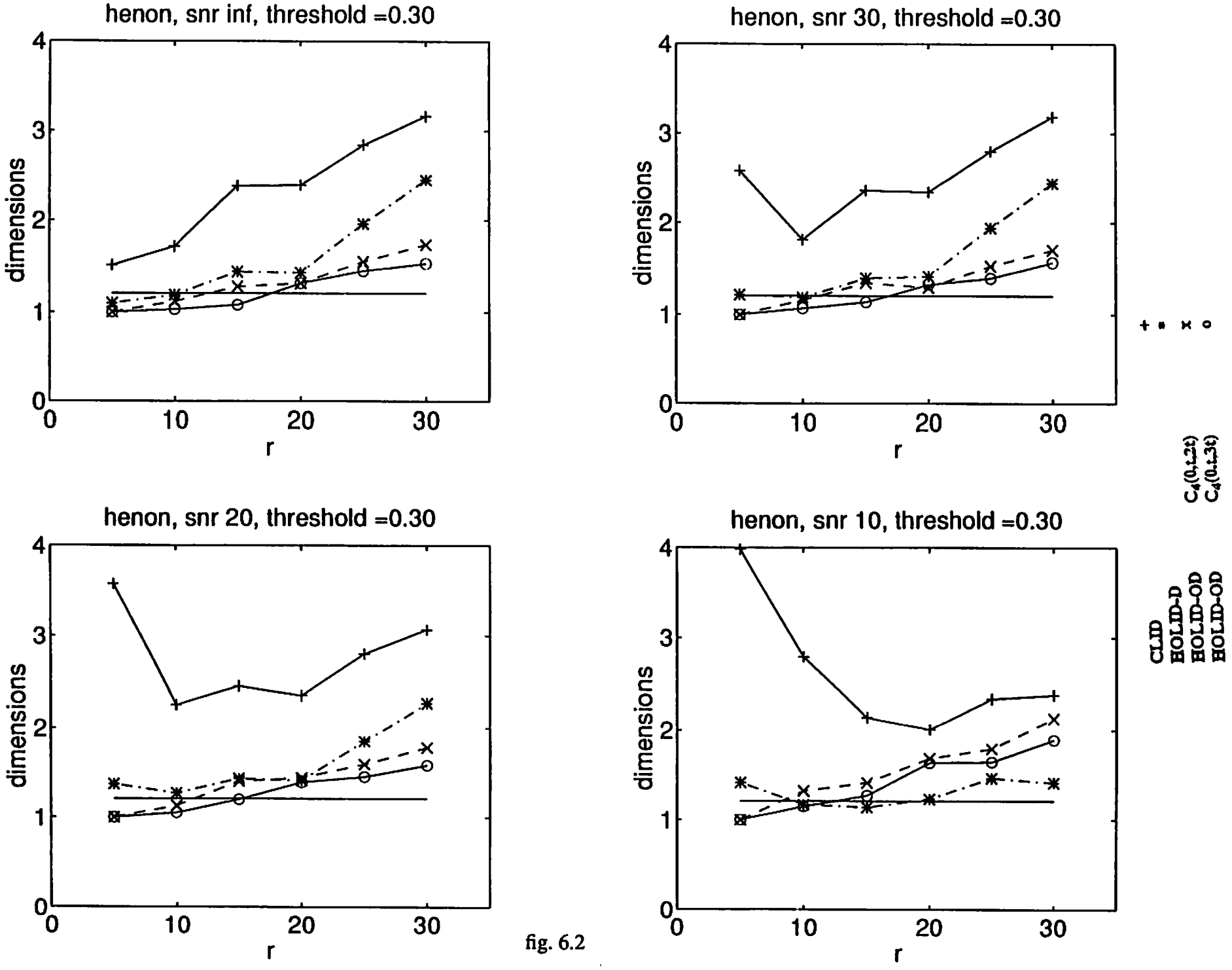
henon, snr inf, threshold =0.30
henon, snr 30, threshold =0.30
henon, snr 20, threshold =0.30
henon, snr 10, threshold =0.30
dimensions
r
0
10
20
30
1
2
3
4
+ * x o
$C_4(0,\pm 2t)$
$C_4(0,\pm 3t)$
CLID
HOLID-D
HOLID-OD
HOLID-OD

fig. 6.2

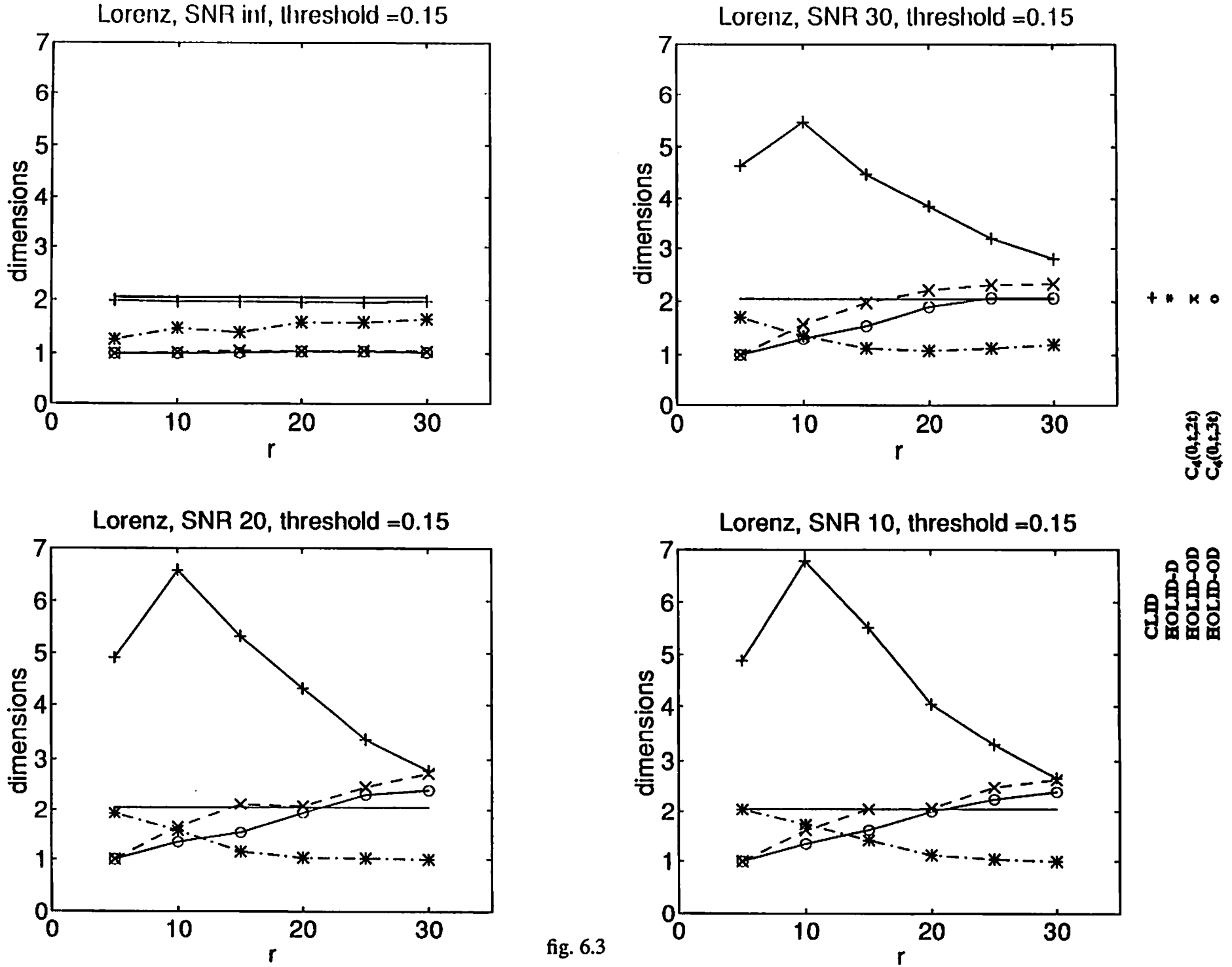
Lorenz, SNR inf, threshold =0.15
Lorenz, SNR 30, threshold =0.15
Lorenz, SNR 20, threshold =0.15
Lorenz, SNR 10, threshold =0.15
dimensions
r
0
10
20
30
1
2
3
4
5
6
7
+ * × o
C4(0,t,2t)
C4(0,t,3t)
CLID
HOLID-D
HOLID-OD
HOLID-OD

fig. 6.3

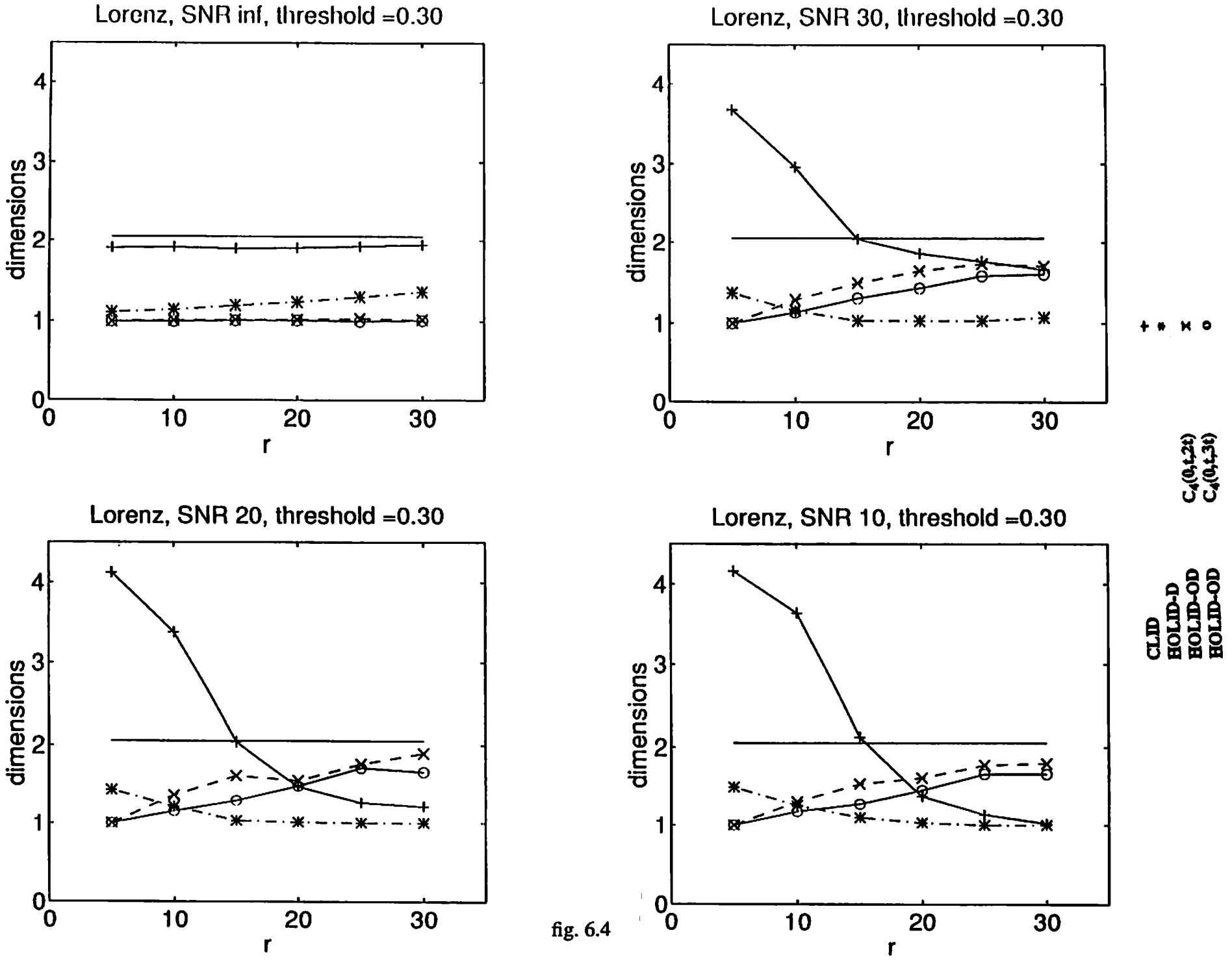
Lorenz, SNR inf, threshold =0.30
Lorenz, SNR 30, threshold =0.30
Lorenz, SNR 20, threshold =0.30
Lorenz, SNR 10, threshold =0.30
dimensions
r
0
10
20
30
1
2
3
4
+ * × o
C4(0,t,2t)
C4(0,t,3t)
CLID
HOLID-D
HOLID-OD
HOLID-OD

fig. 6.4

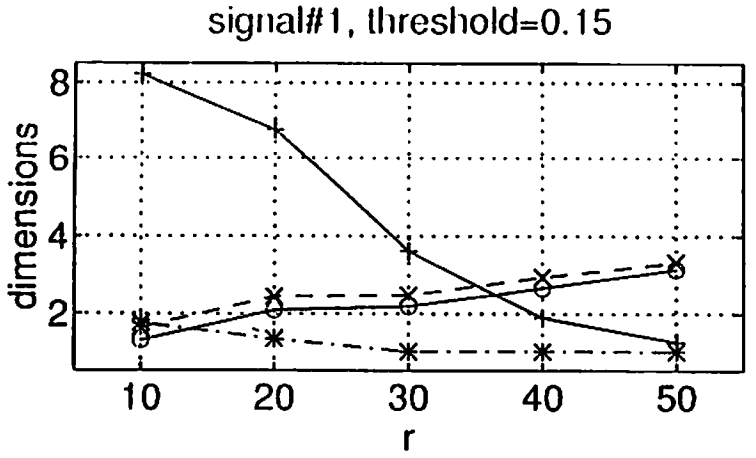
signal#1, threshold=0.15
dimensions
r
8
6
4
2
10
20
30
40
50

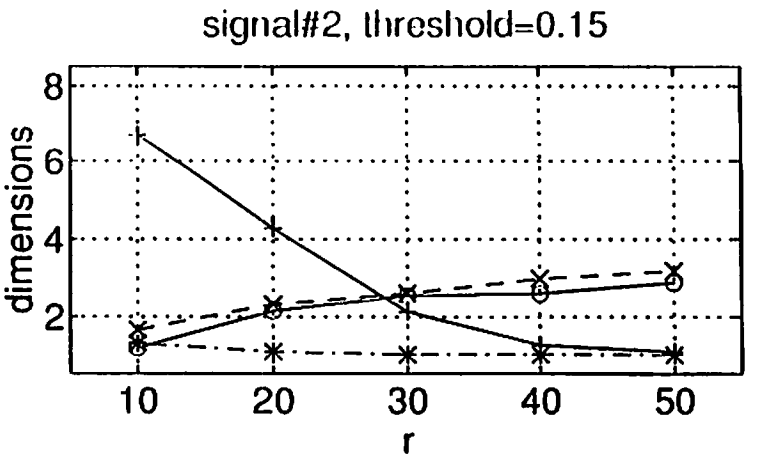
signal#2, threshold=0.15
dimensions
r
8
6
4
2
10
20
30
40
50

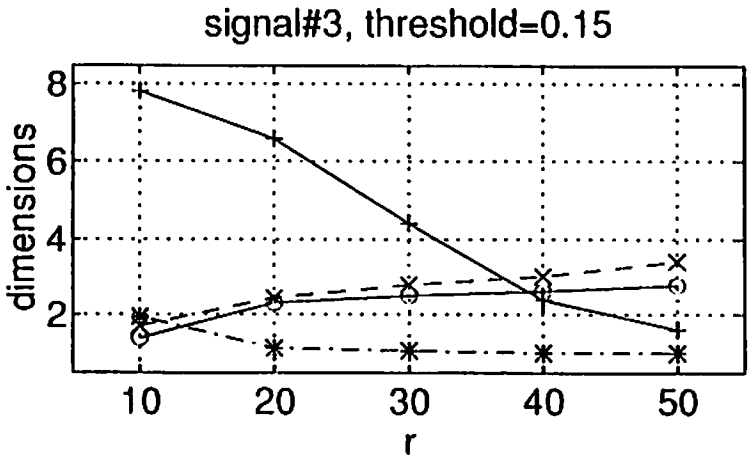
signal#3, threshold=0.15
dimensions
r
8
6
4
2
10
20
30
40
50

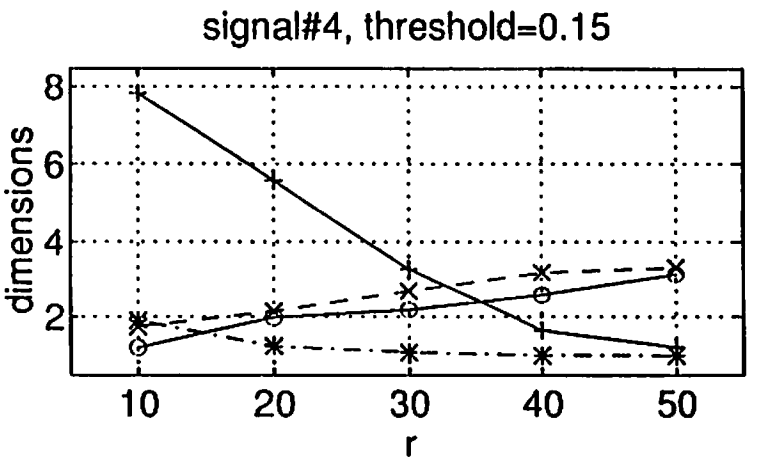
signal#4, threshold=0.15
dimensions
r
8
6
4
2
10
20
30
40
50

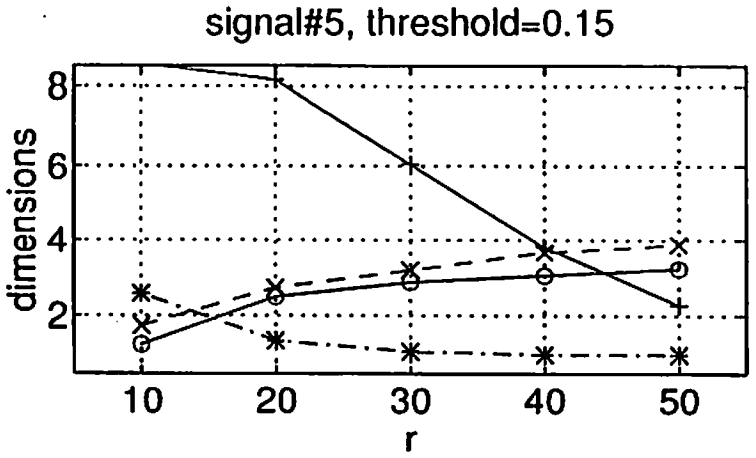
signal#5, threshold=0.15
dimensions
r
8
6
4
2
10
20
30
40
50

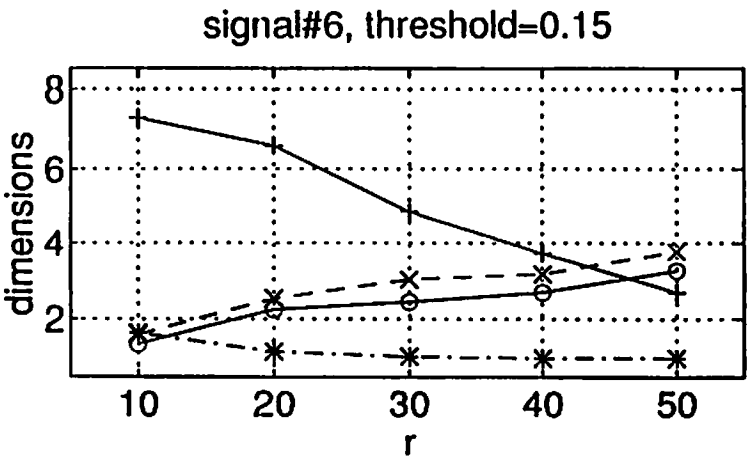
signal#6, threshold=0.15
dimensions
r
8
6
4
2
10
20
30
40
50

fig. 6.5

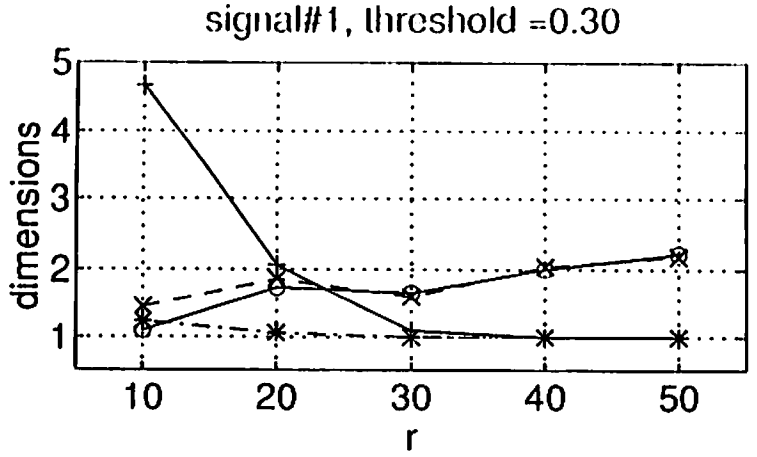
signal#1, threshold =0.30
dimensions
r
1
2
3
4
5
10
20
30
40
50

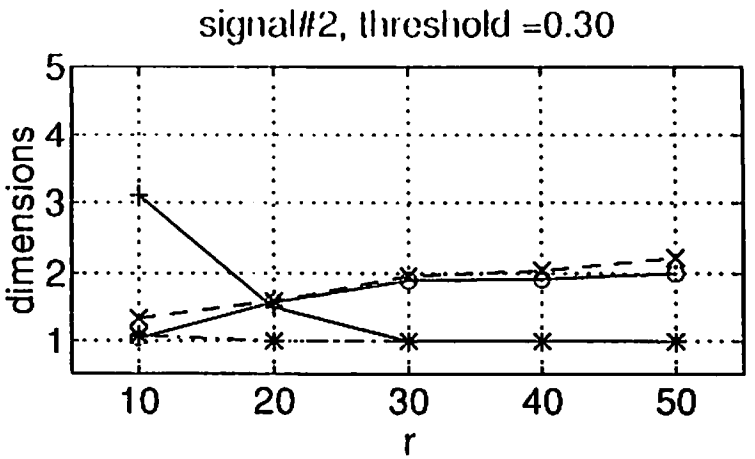
signal#2, threshold =0.30
dimensions
r
1
2
3
4
5
10
20
30
40
50

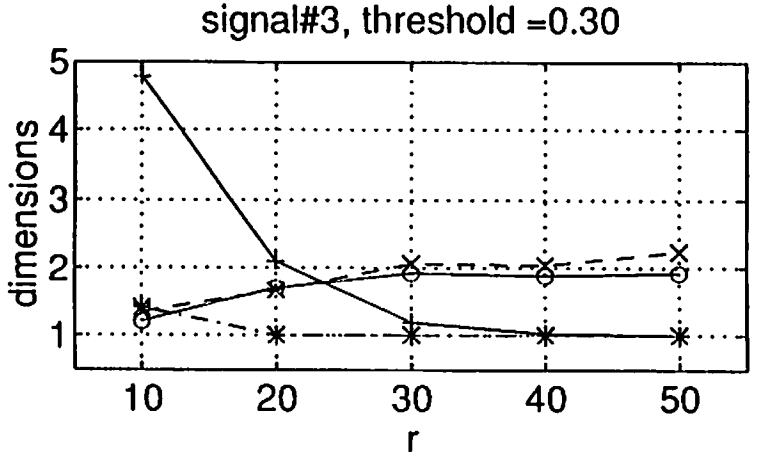
signal#3, threshold =0.30
dimensions
r
1
2
3
4
5
10
20
30
40
50

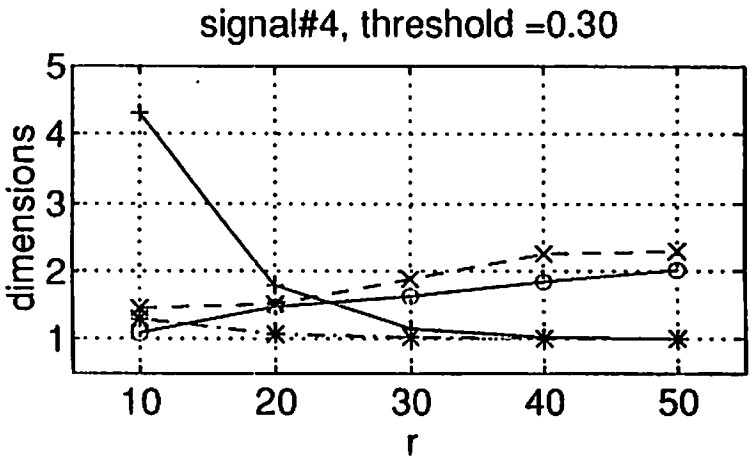
signal#4, threshold =0.30
dimensions
r
1
2
3
4
5
10
20
30
40
50

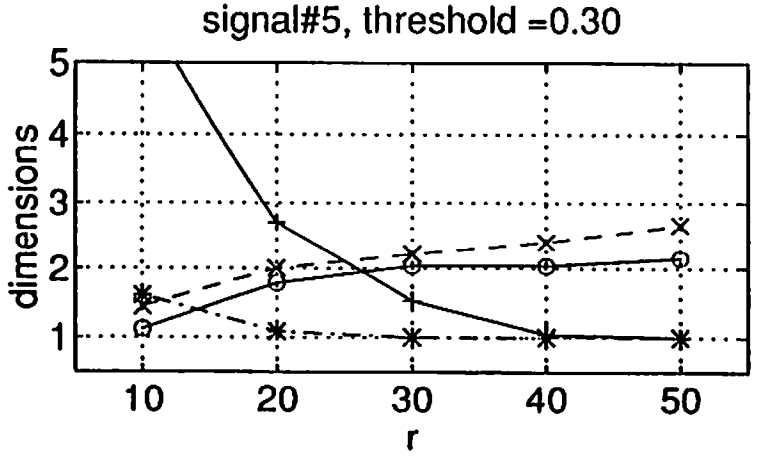
signal#5, threshold =0.30
dimensions
r
1
2
3
4
5
10
20
30
40
50

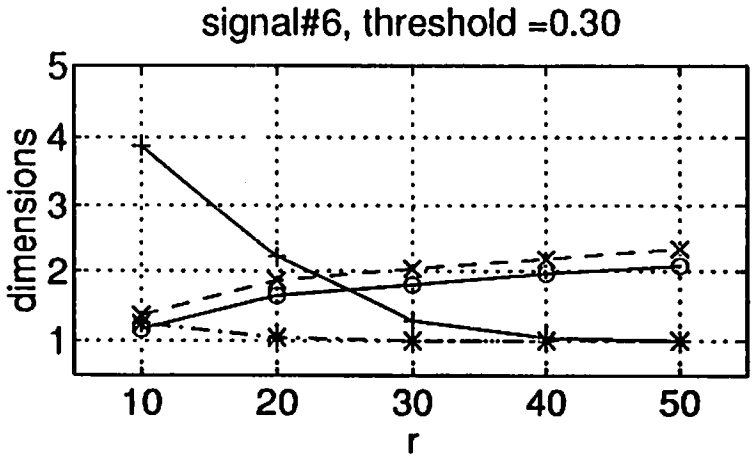
signal#6, threshold =0.30
dimensions
r
1
2
3
4
5
10
20
30
40
50

fig. 6.6

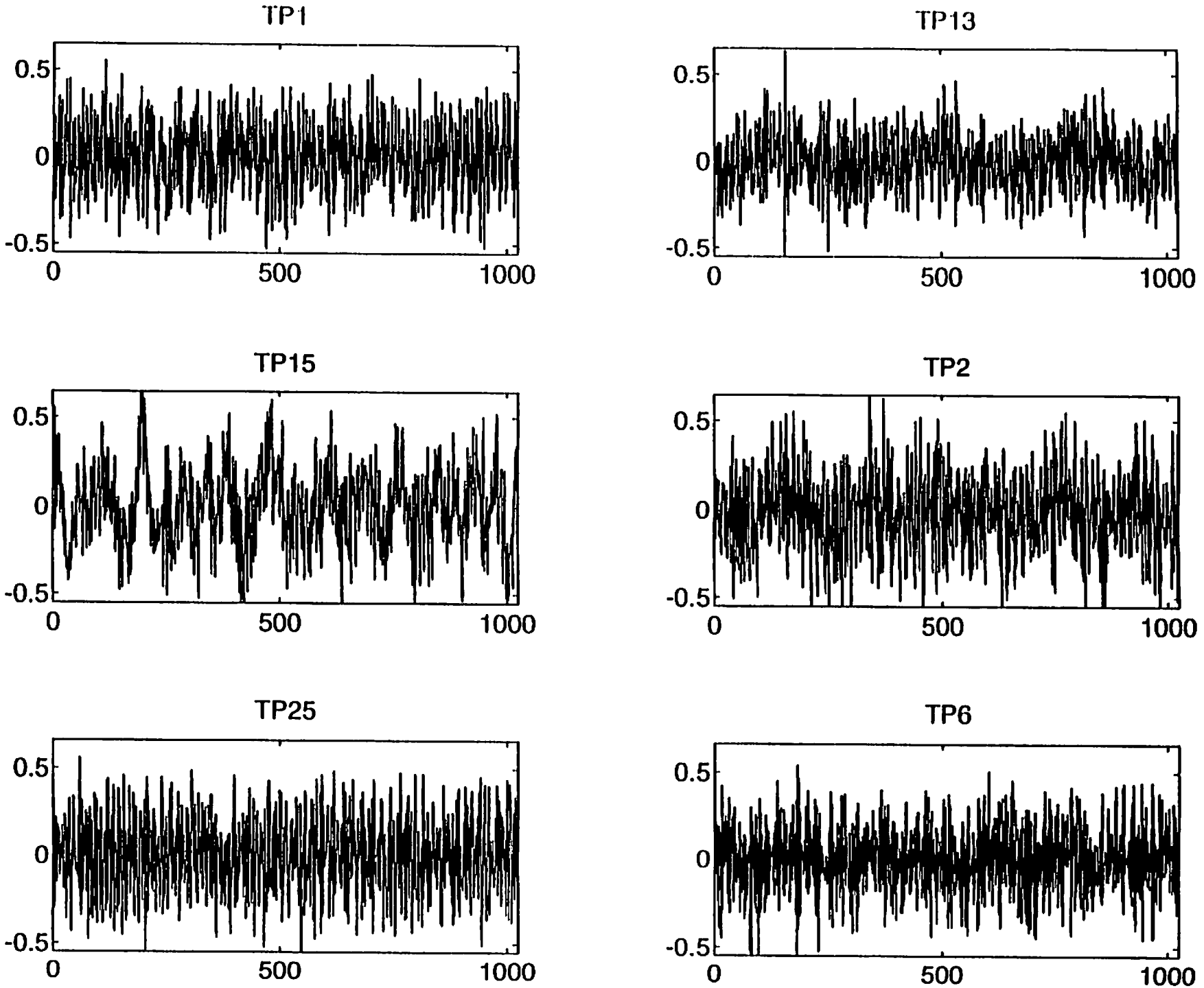


fig. 7.1

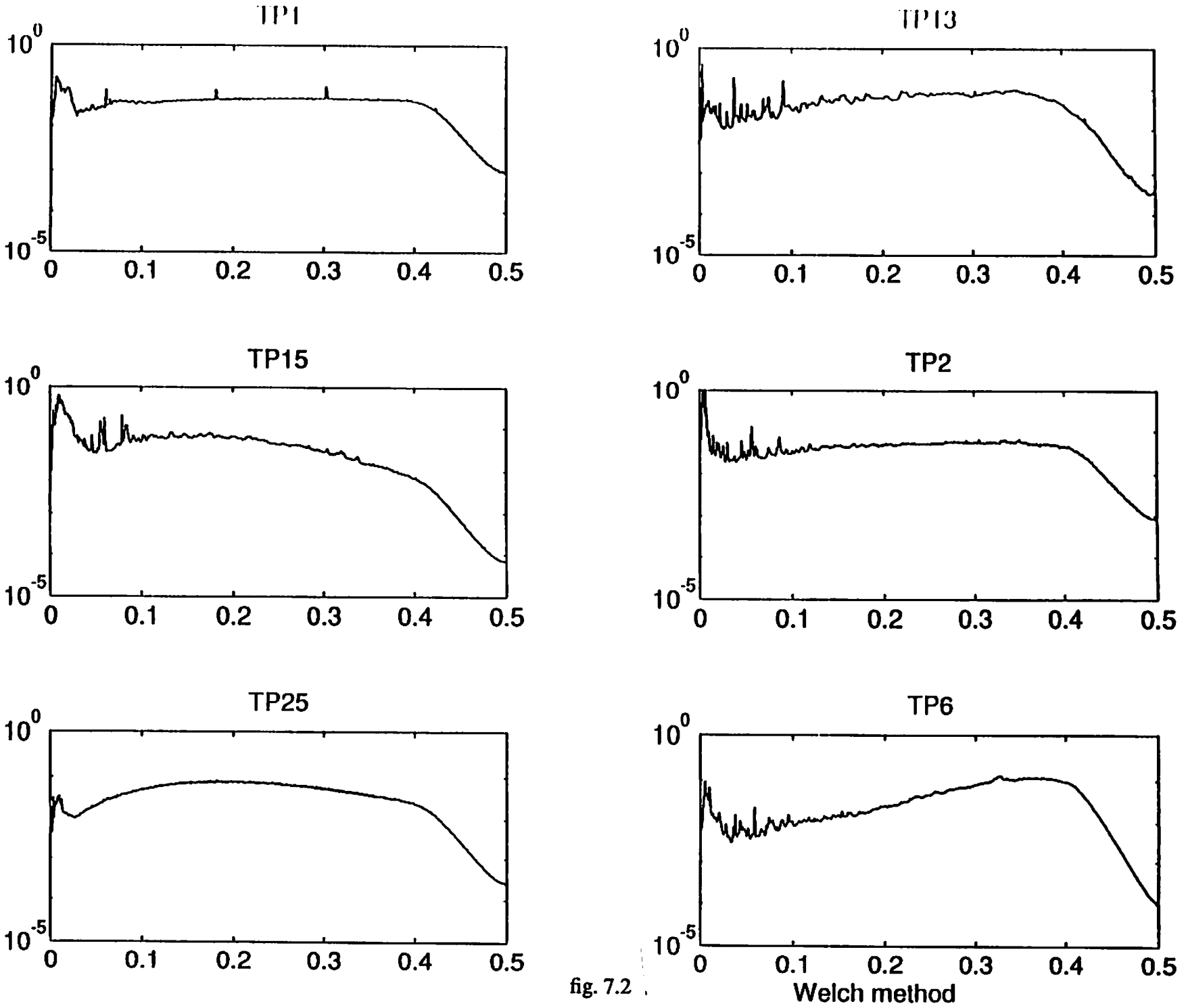


fig. 7.2

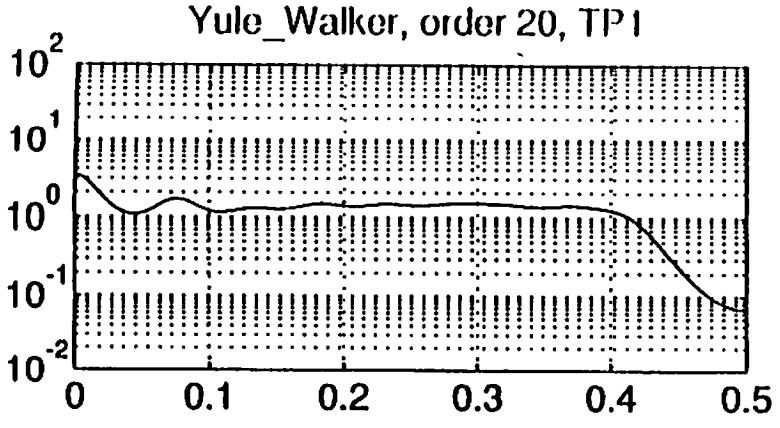
Yule_Walker, order 20, TP1
$10^2$
$10^1$
$10^0$
$10^{-1}$
$10^{-2}$
0
0.1
0.2
0.3
0.4
0.5

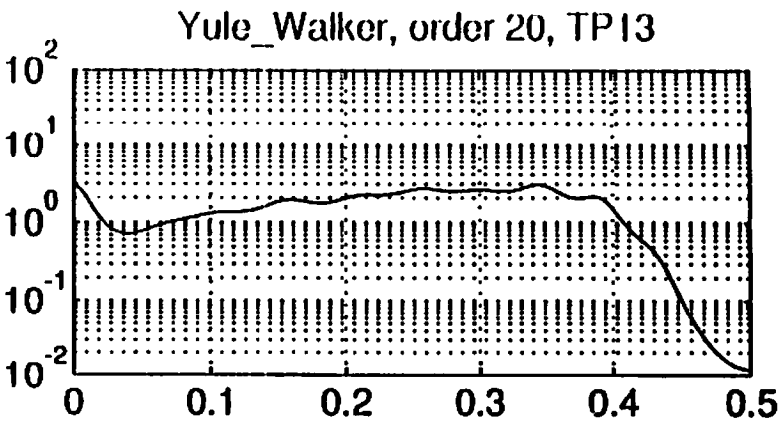
Yule_Walker, order 20, TP13
$10^2$
$10^1$
$10^0$
$10^{-1}$
$10^{-2}$
0
0.1
0.2
0.3
0.4
0.5

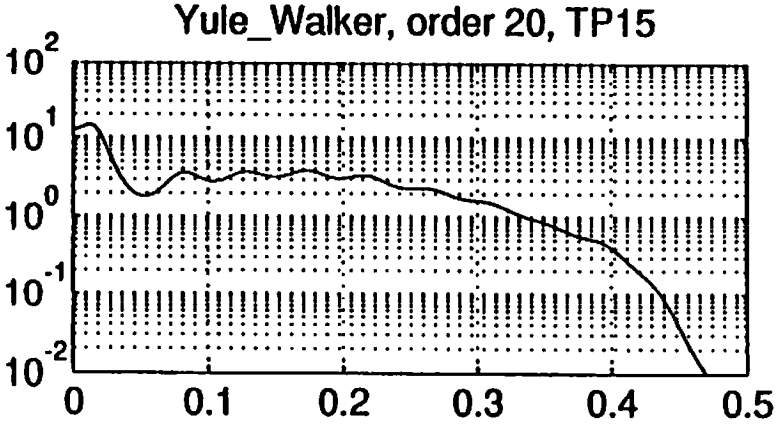
Yule_Walker, order 20, TP15
$10^2$
$10^1$
$10^0$
$10^{-1}$
$10^{-2}$
0
0.1
0.2
0.3
0.4
0.5

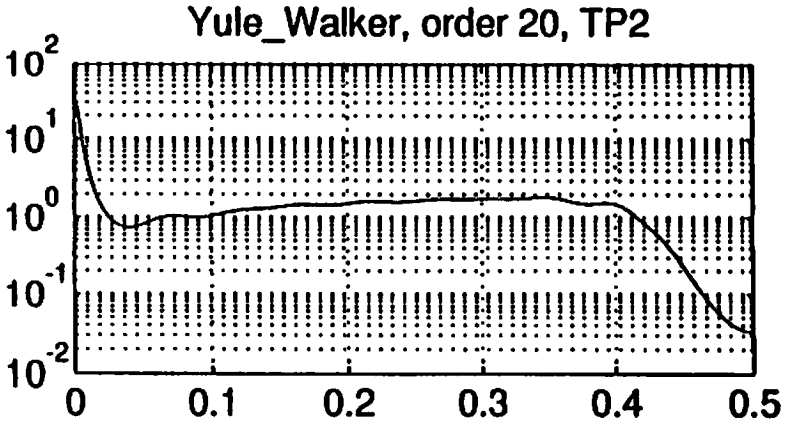
Yule_Walker, order 20, TP2
$10^2$
$10^1$
$10^0$
$10^{-1}$
$10^{-2}$
0
0.1
0.2
0.3
0.4
0.5

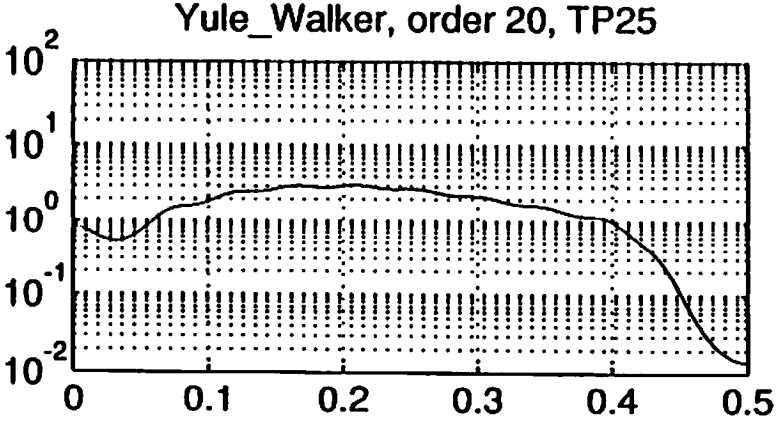
Yule_Walker, order 20, TP25
$10^2$
$10^1$
$10^0$
$10^{-1}$
$10^{-2}$
0
0.1
0.2
0.3
0.4
0.5

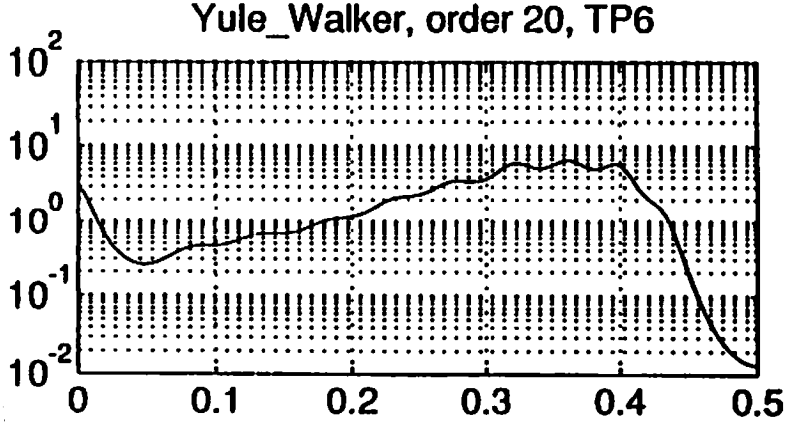
Yule_Walker, order 20, TP6
$10^2$
$10^1$
$10^0$
$10^{-1}$
$10^{-2}$
0
0.1
0.2
0.3
0.4
0.5

fig. 7.3

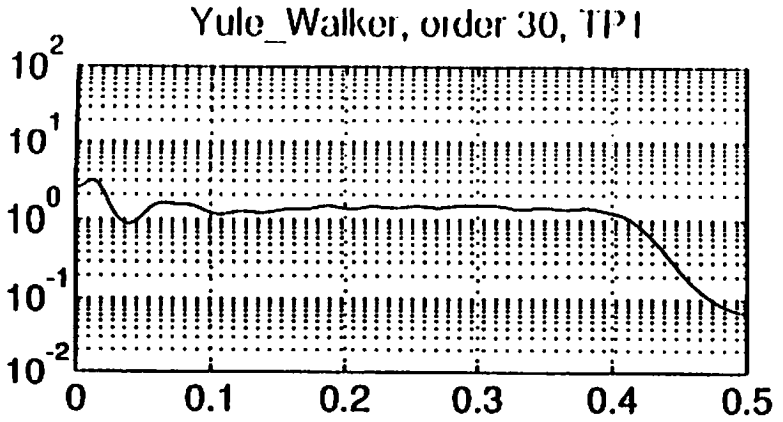
Yule_Walker, order 30, TP1
$10^2$
$10^1$
$10^0$
$10^{-1}$
$10^{-2}$
0
0.1
0.2
0.3
0.4
0.5

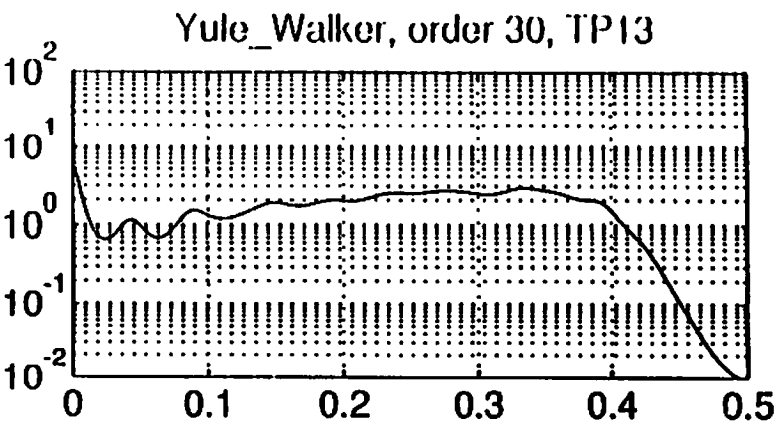
Yule_Walker, order 30, TP13
$10^2$
$10^1$
$10^0$
$10^{-1}$
$10^{-2}$
0
0.1
0.2
0.3
0.4
0.5

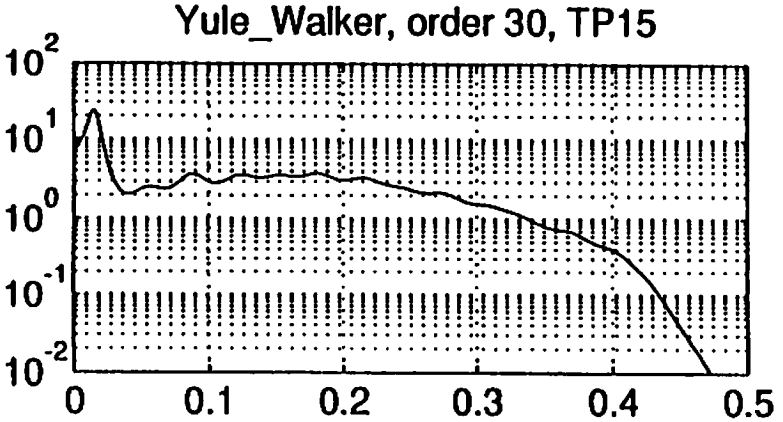
Yule_Walker, order 30, TP15
$10^2$
$10^1$
$10^0$
$10^{-1}$
$10^{-2}$
0
0.1
0.2
0.3
0.4
0.5

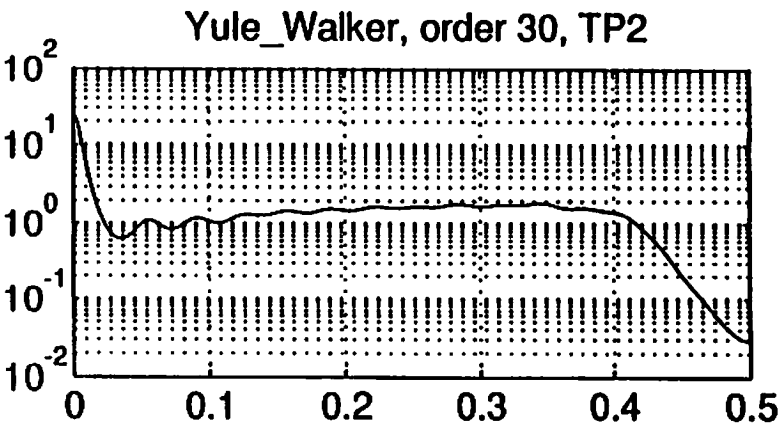
Yule_Walker, order 30, TP2
$10^2$
$10^1$
$10^0$
$10^{-1}$
$10^{-2}$
0
0.1
0.2
0.3
0.4
0.5

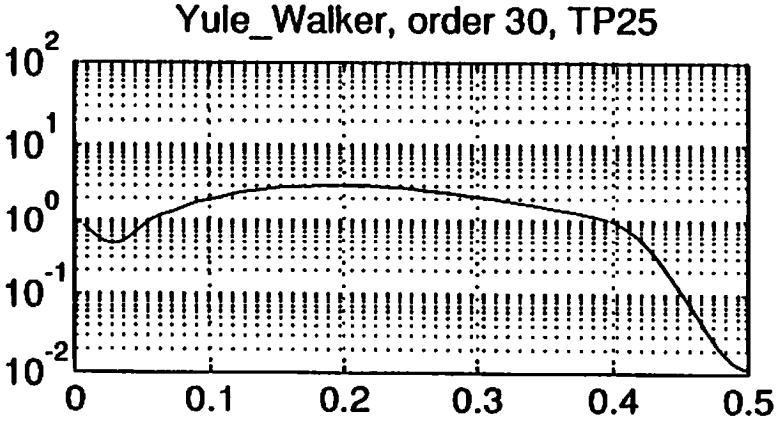
Yule_Walker, order 30, TP25
$10^2$
$10^1$
$10^0$
$10^{-1}$
$10^{-2}$
0
0.1
0.2
0.3
0.4
0.5

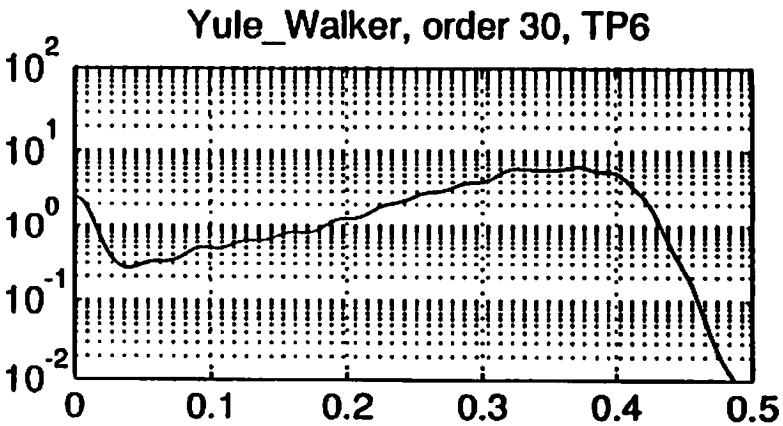
Yule_Walker, order 30, TP6
$10^2$
$10^1$
$10^0$
$10^{-1}$
$10^{-2}$
0
0.1
0.2
0.3
0.4
0.5

fig. 7.4

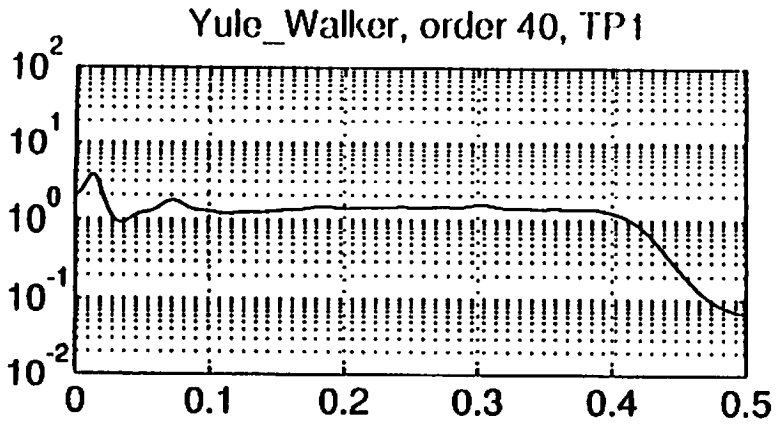
Yule_Walker, order 40, TP1
$10^2$
$10^1$
$10^0$
$10^{-1}$
$10^{-2}$
0
0.1
0.2
0.3
0.4
0.5

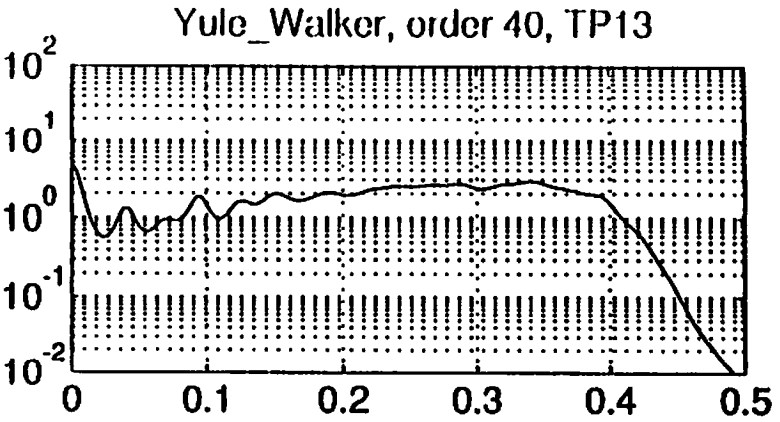
Yule_Walker, order 40, TP13
$10^2$
$10^1$
$10^0$
$10^{-1}$
$10^{-2}$
0
0.1
0.2
0.3
0.4
0.5

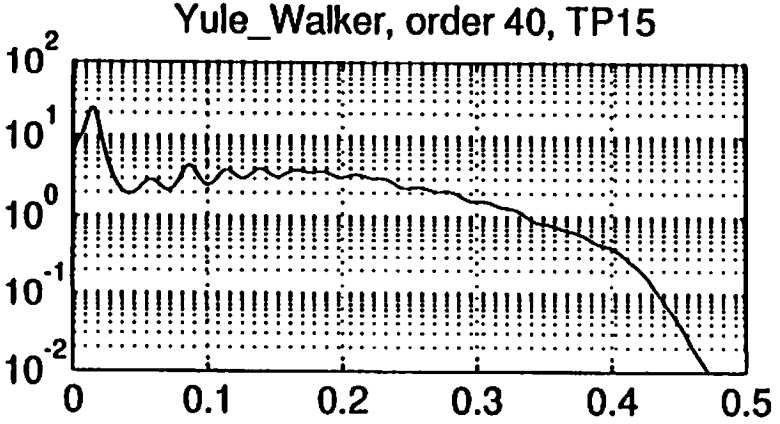
Yule_Walker, order 40, TP15
$10^2$
$10^1$
$10^0$
$10^{-1}$
$10^{-2}$
0
0.1
0.2
0.3
0.4
0.5

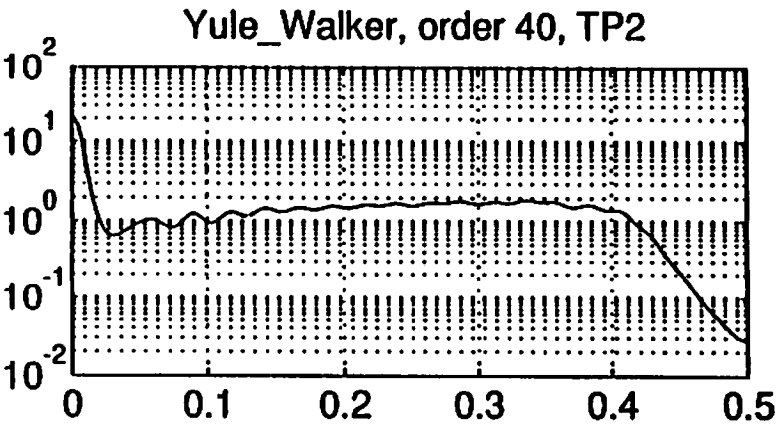
Yule_Walker, order 40, TP2
$10^2$
$10^1$
$10^0$
$10^{-1}$
$10^{-2}$
0
0.1
0.2
0.3
0.4
0.5

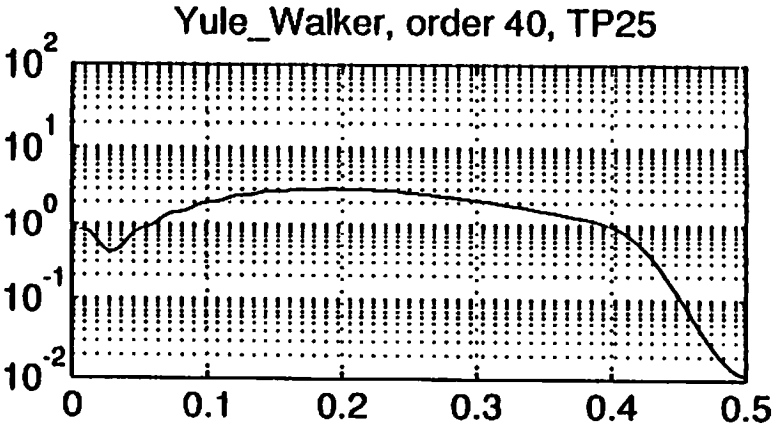
Yule_Walker, order 40, TP25
$10^2$
$10^1$
$10^0$
$10^{-1}$
$10^{-2}$
0
0.1
0.2
0.3
0.4
0.5

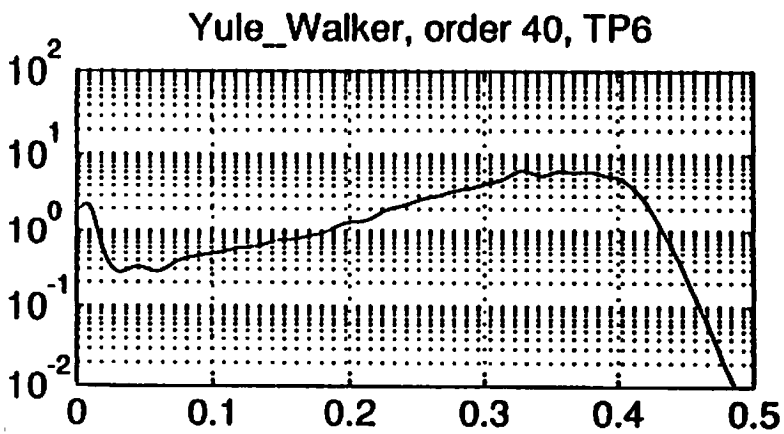
Yule_Walker, order 40, TP6
$10^2$
$10^1$
$10^0$
$10^{-1}$
$10^{-2}$
0
0.1
0.2
0.3
0.4
0.5

fig. 7.5

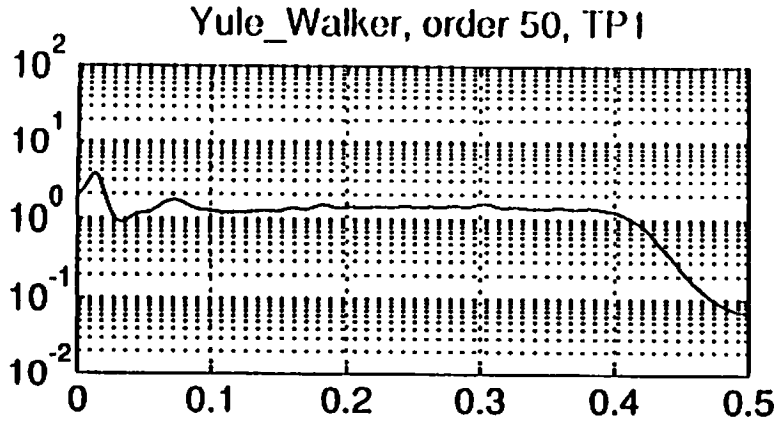
Yule_Walker, order 50, TP1
$10^2$
$10^1$
$10^0$
$10^{-1}$
$10^{-2}$
0
0.1
0.2
0.3
0.4
0.5

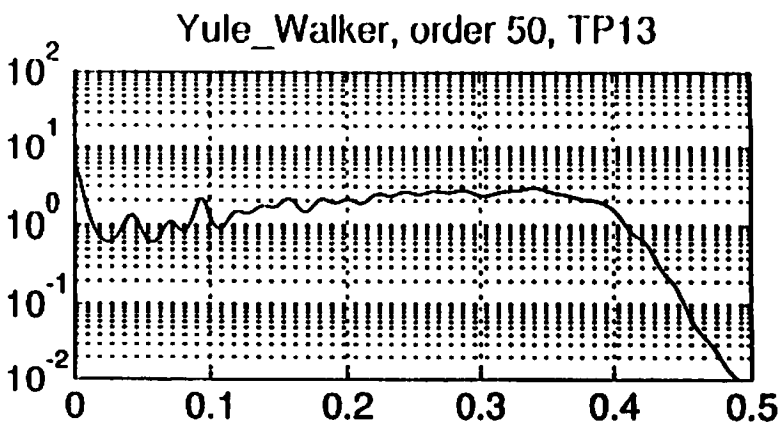
Yule_Walker, order 50, TP13
$10^2$
$10^1$
$10^0$
$10^{-1}$
$10^{-2}$
0
0.1
0.2
0.3
0.4
0.5

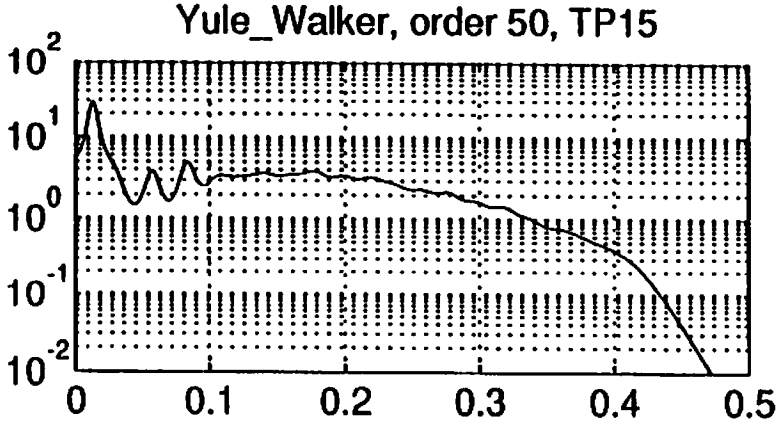
Yule_Walker, order 50, TP15
$10^2$
$10^1$
$10^0$
$10^{-1}$
$10^{-2}$
0
0.1
0.2
0.3
0.4
0.5

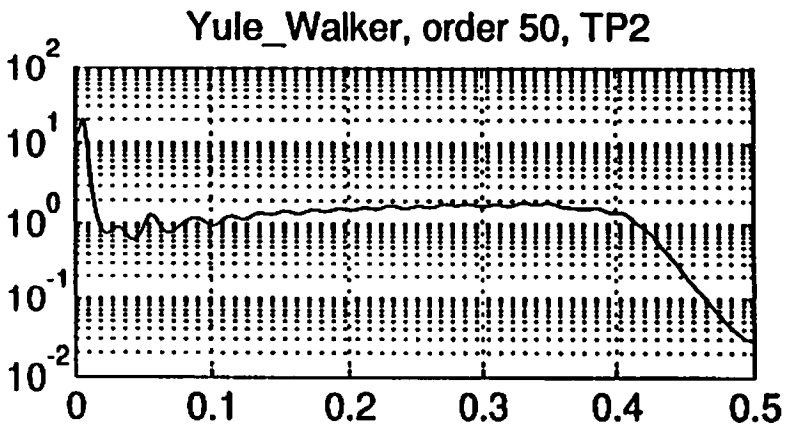
Yule_Walker, order 50, TP2
$10^2$
$10^1$
$10^0$
$10^{-1}$
$10^{-2}$
0
0.1
0.2
0.3
0.4
0.5

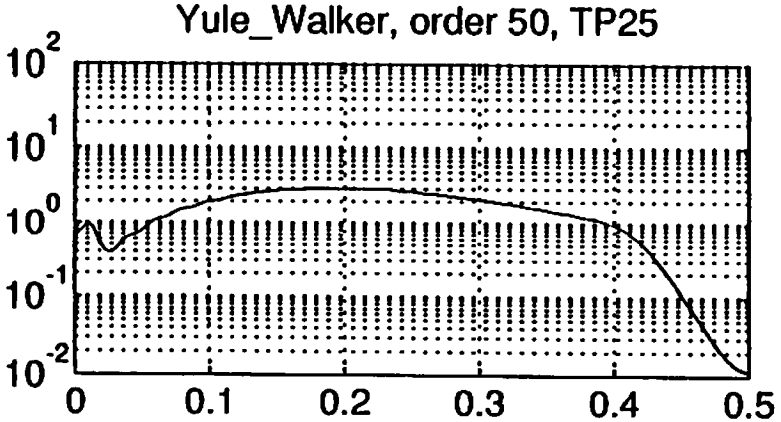
Yule_Walker, order 50, TP25
$10^2$
$10^1$
$10^0$
$10^{-1}$
$10^{-2}$
0
0.1
0.2
0.3
0.4
0.5

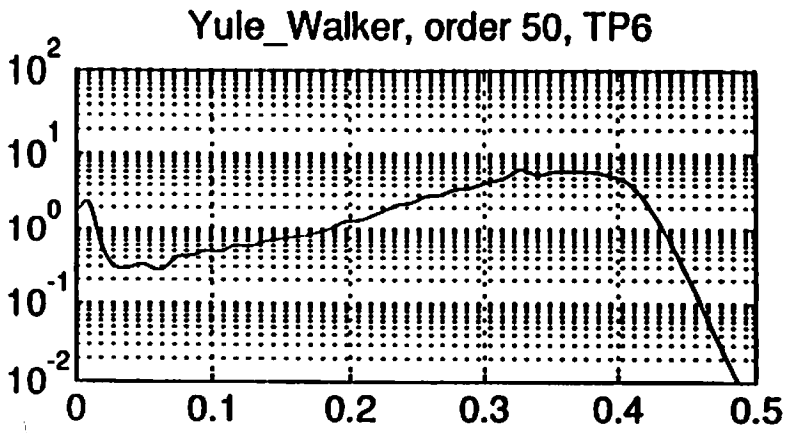
Yule_Walker, order 50, TP6
$10^2$
$10^1$
$10^0$
$10^{-1}$
$10^{-2}$
0
0.1
0.2
0.3
0.4
0.5

fig. 7.6

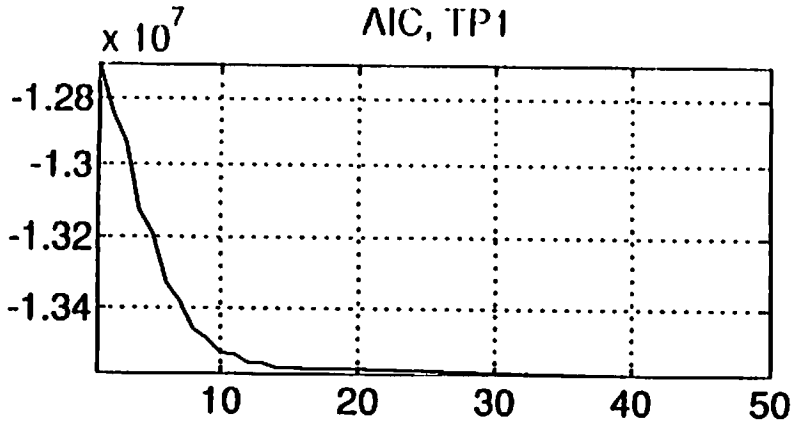
AIC, TP1
x 10^7
-1.28
-1.3
-1.32
-1.34
10
20
30
40
50

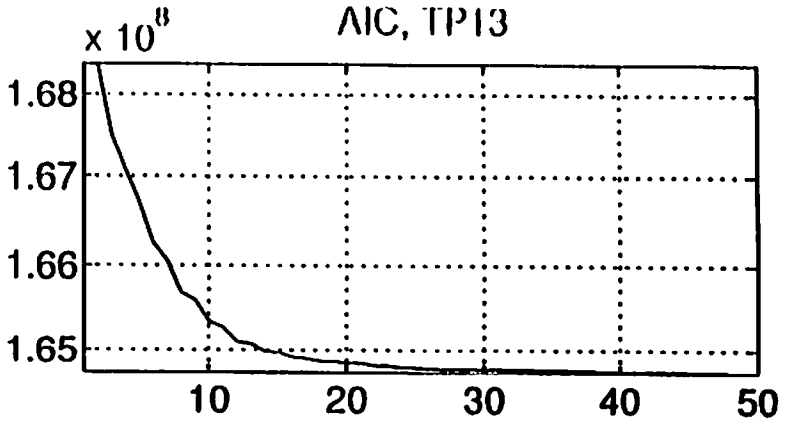
AIC, TP13
x 10^8
1.68
1.67
1.66
1.65
10
20
30
40
50

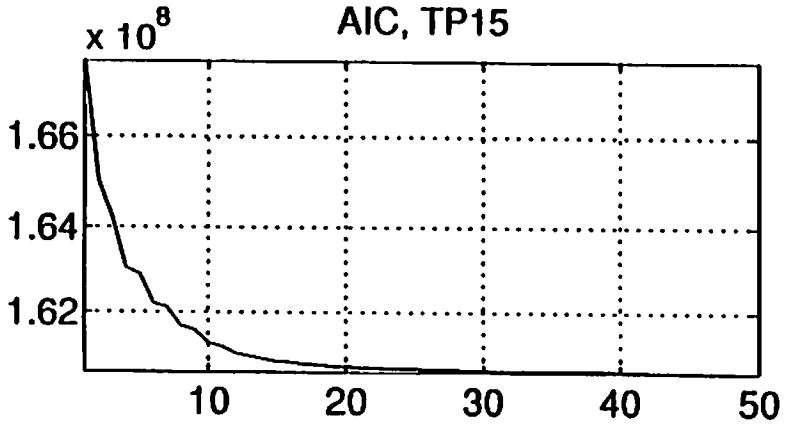
AIC, TP15
x 10^8
1.66
1.64
1.62
10
20
30
40
50

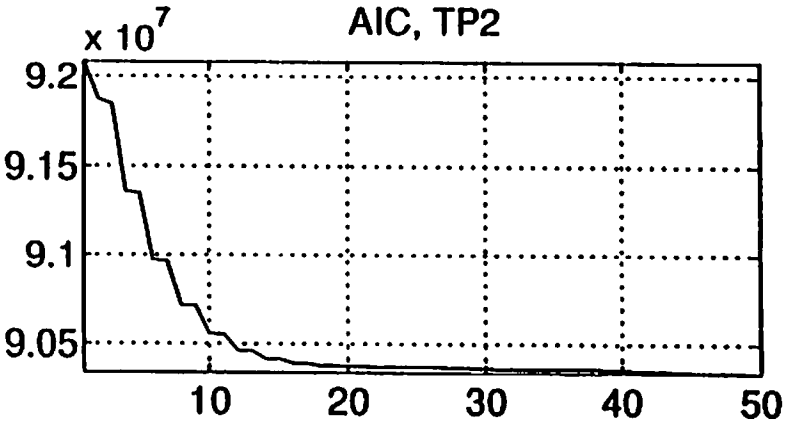
AIC, TP2
x 10^7
9.2
9.15
9.1
9.05
10
20
30
40
50

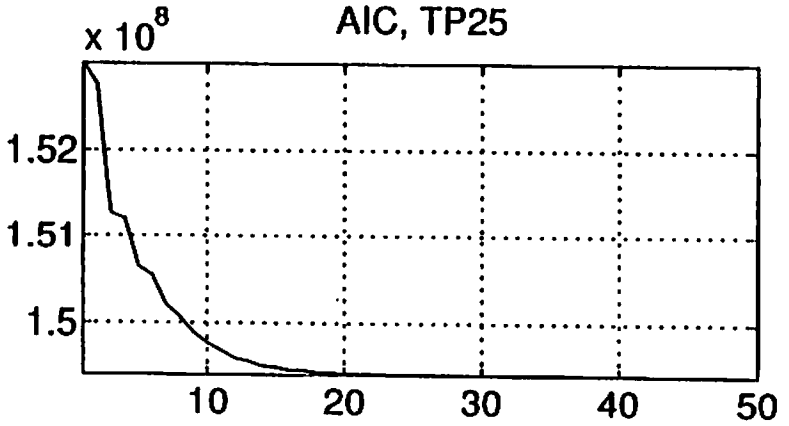
AIC, TP25
x 10^8
1.52
1.51
1.5
10
20
30
40
50

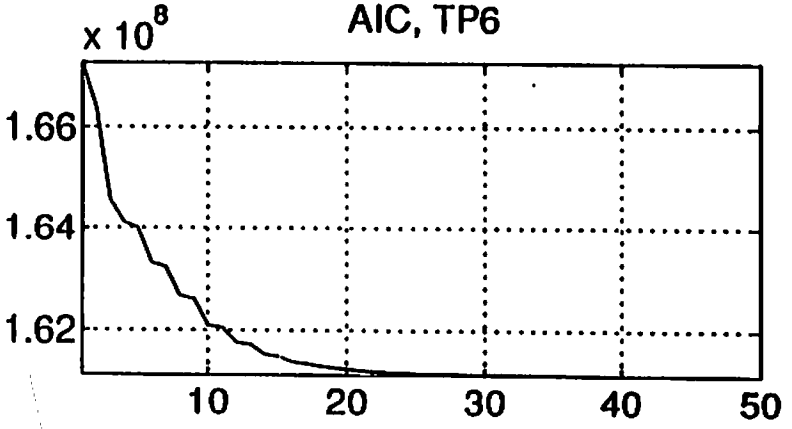
AIC, TP6
x 10^8
1.66
1.64
1.62
10
20
30
40
50

fig. 7.7

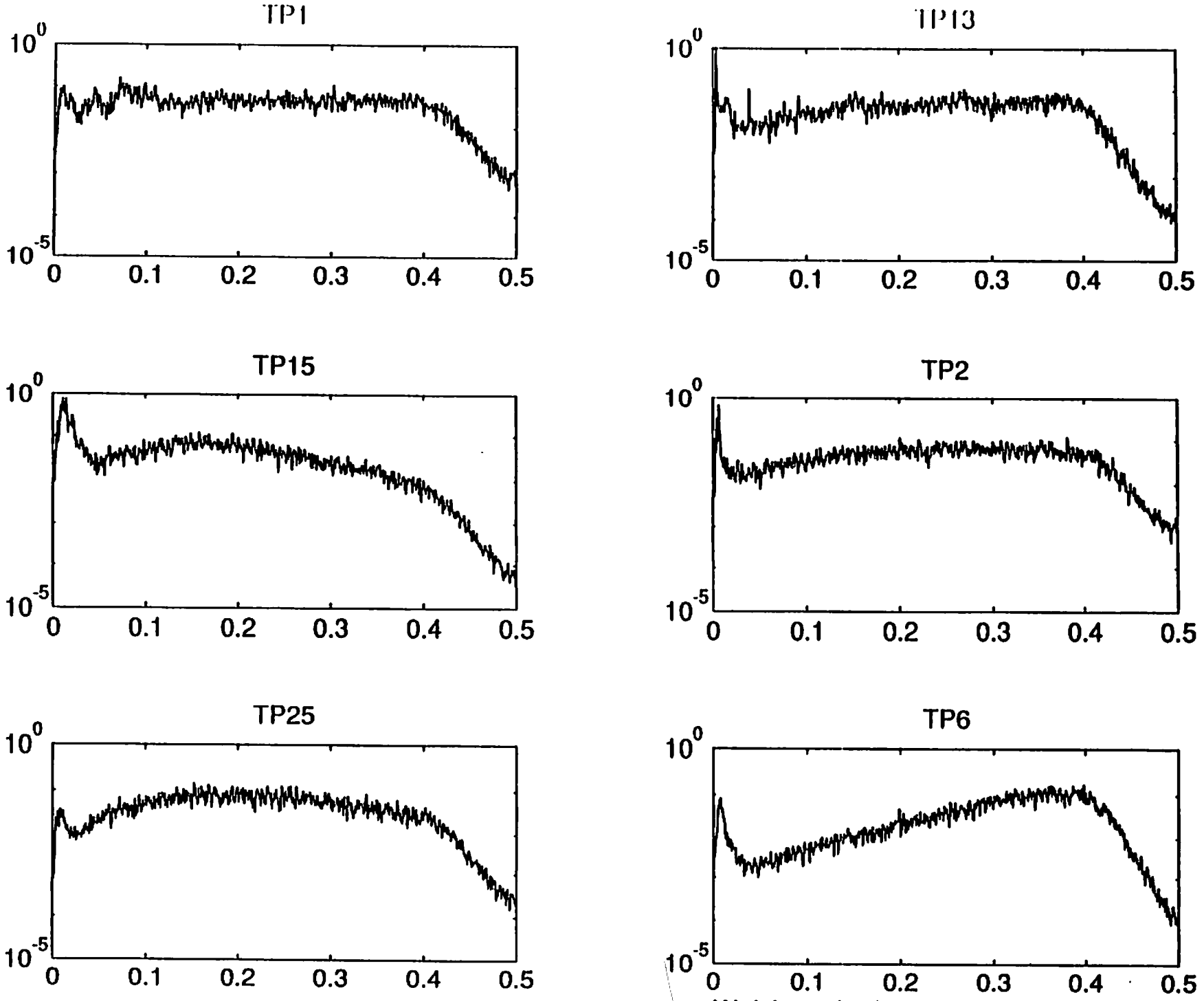


fig. 7.8 Welch method using 32768 samples

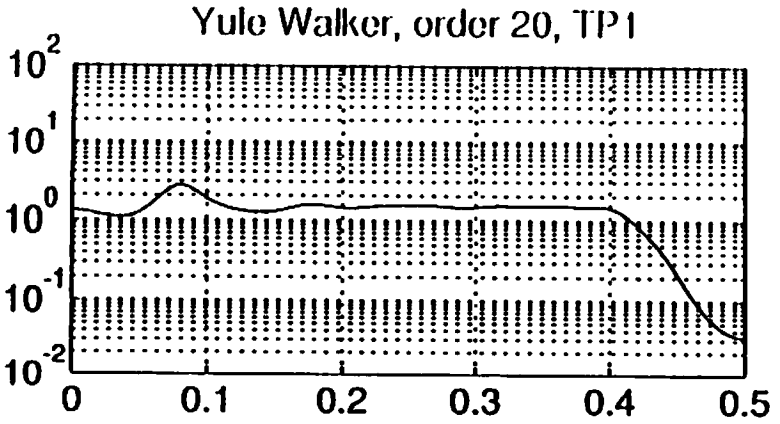


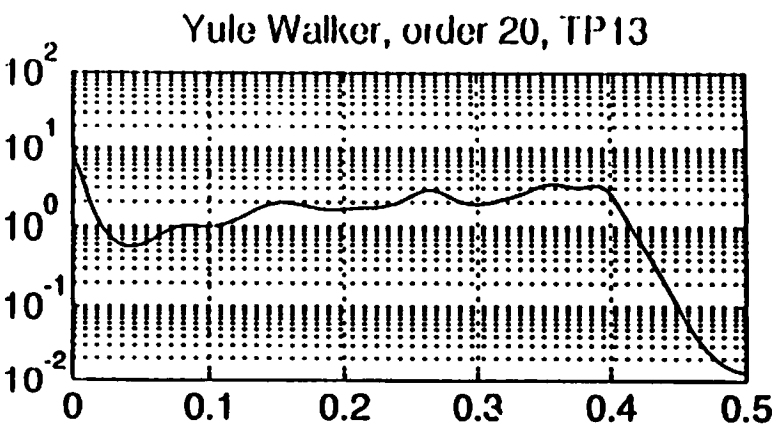


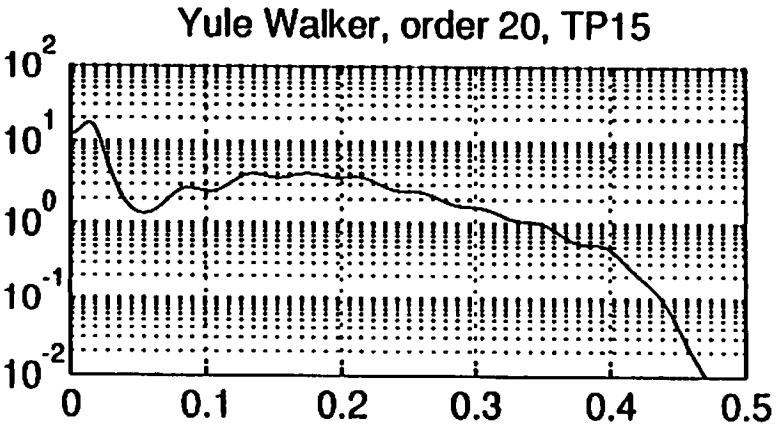


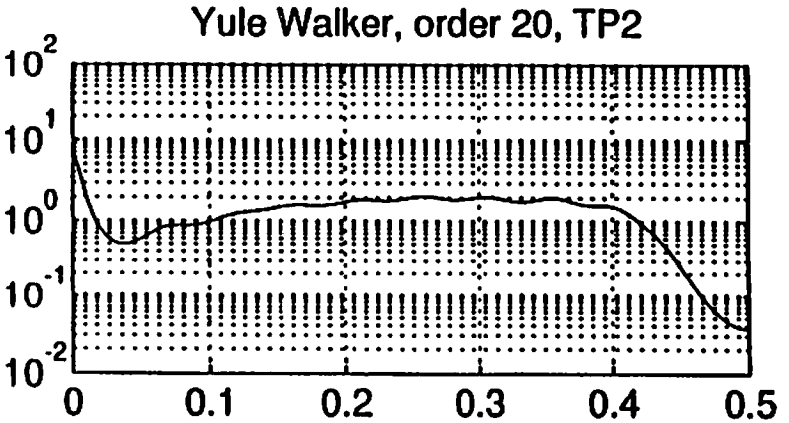


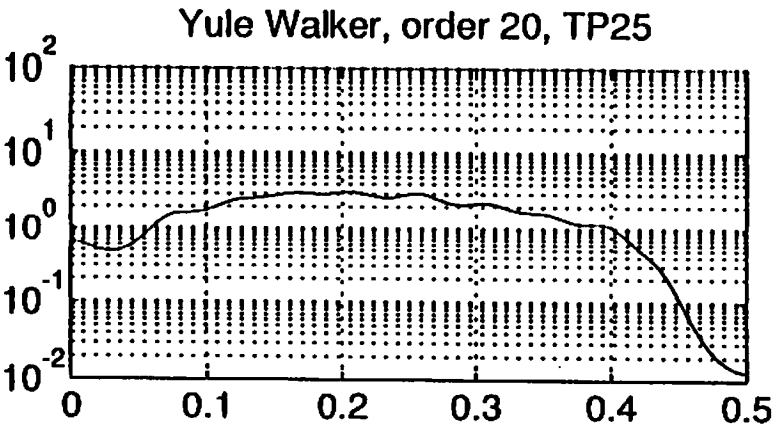


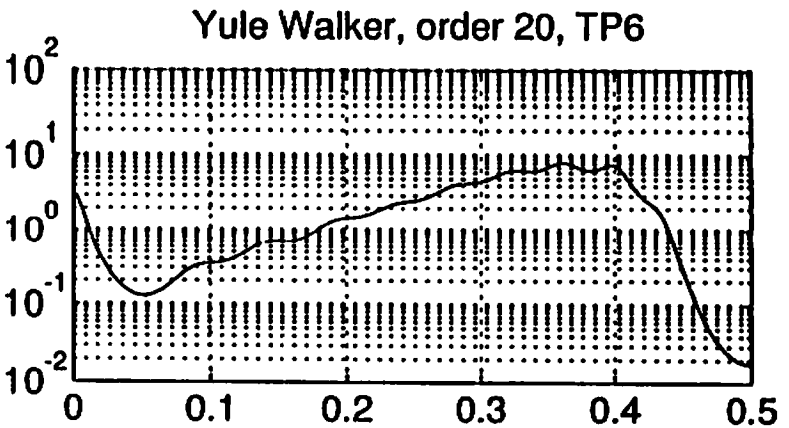


fig. 7.9

using 32768 samples

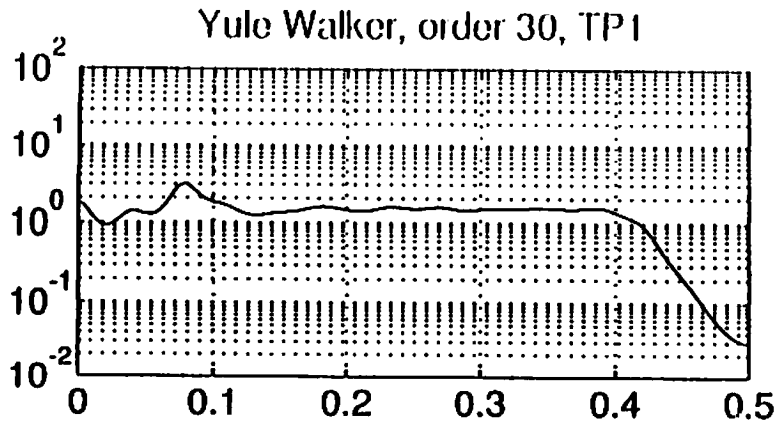


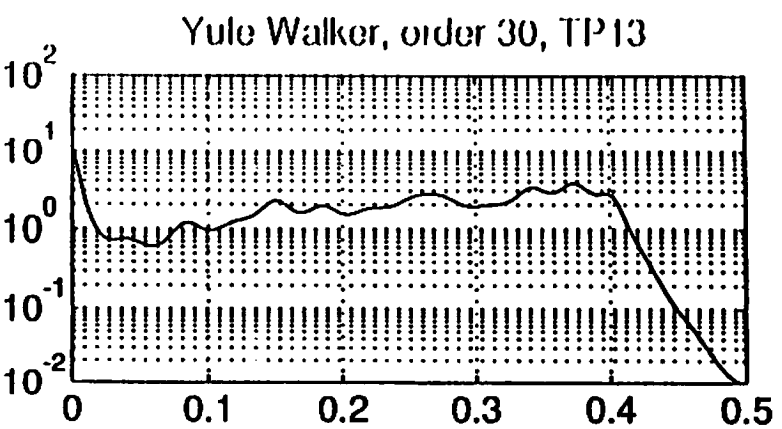


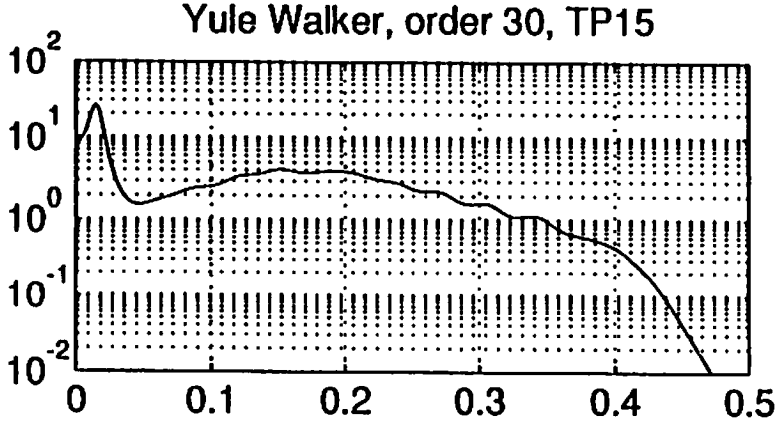


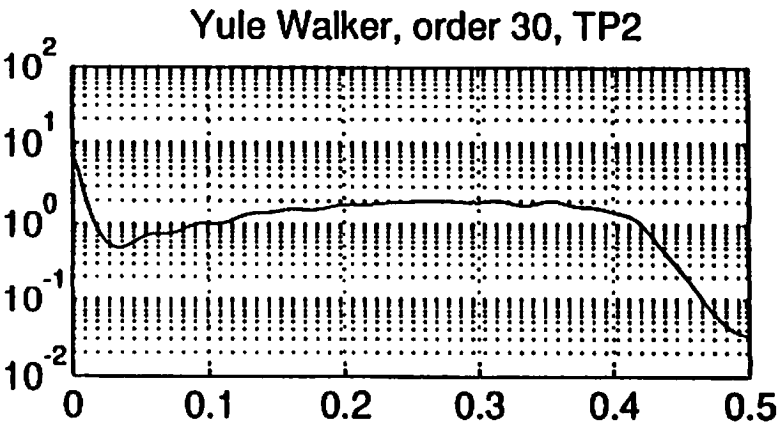


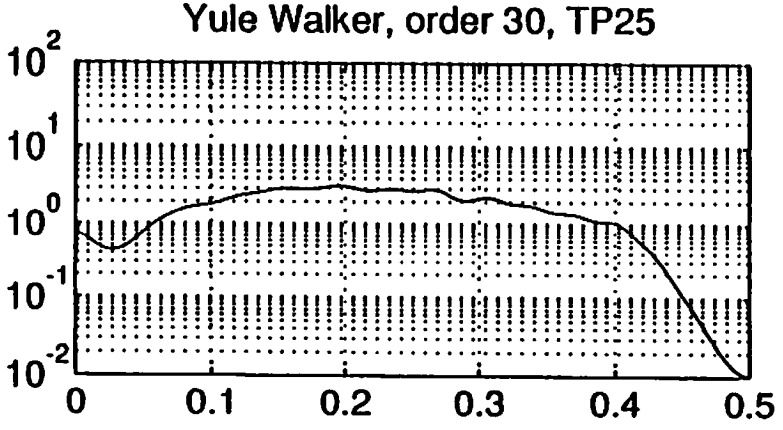


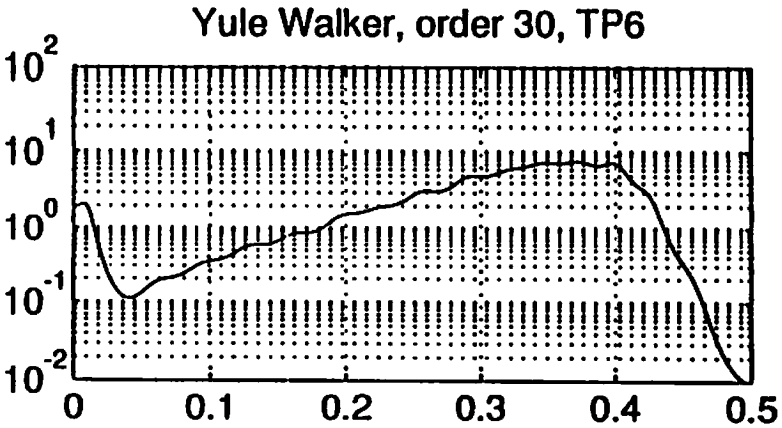


fig. 7.10

using 32768 samples

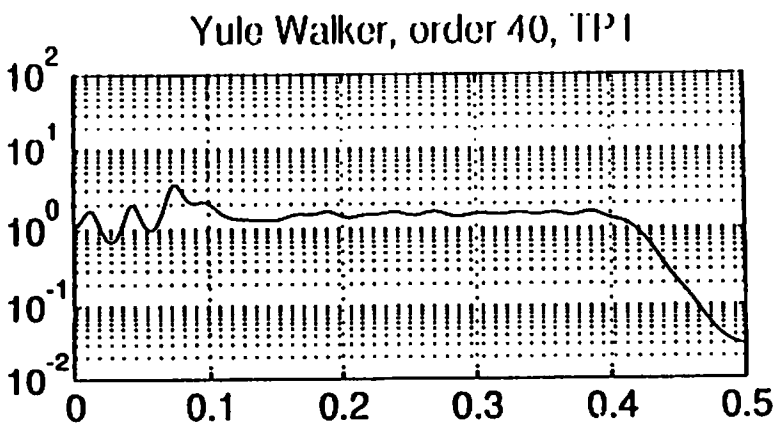


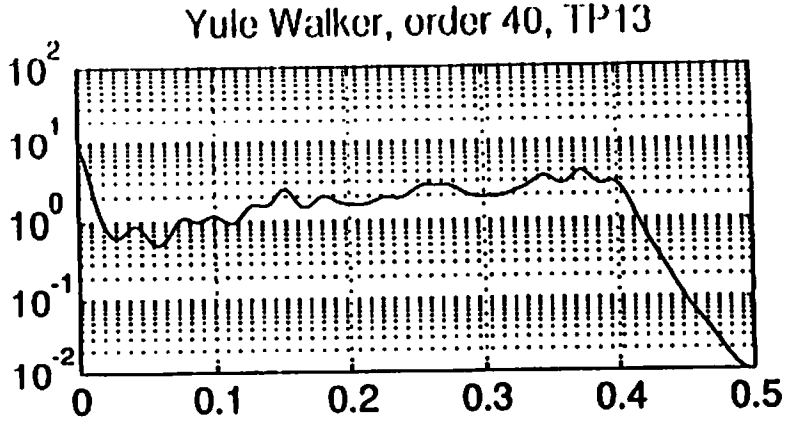


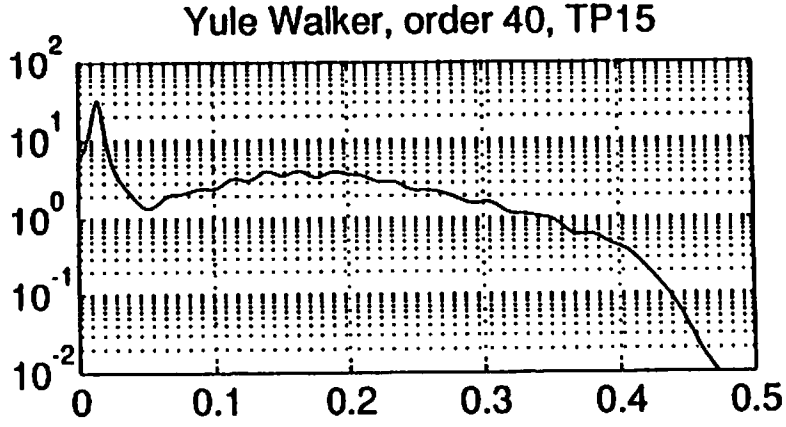


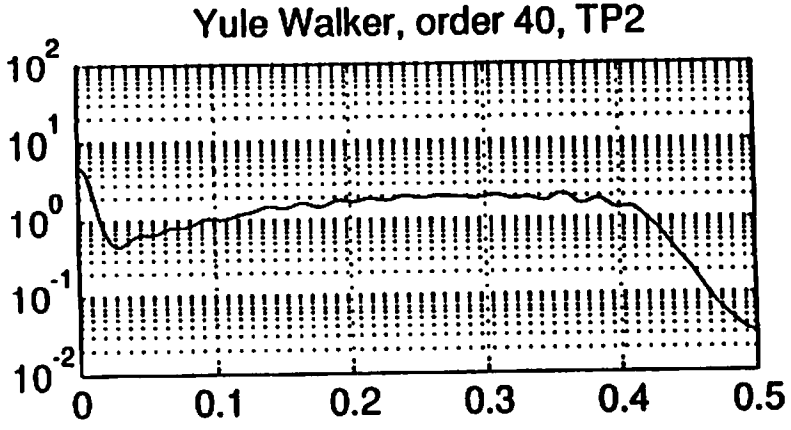


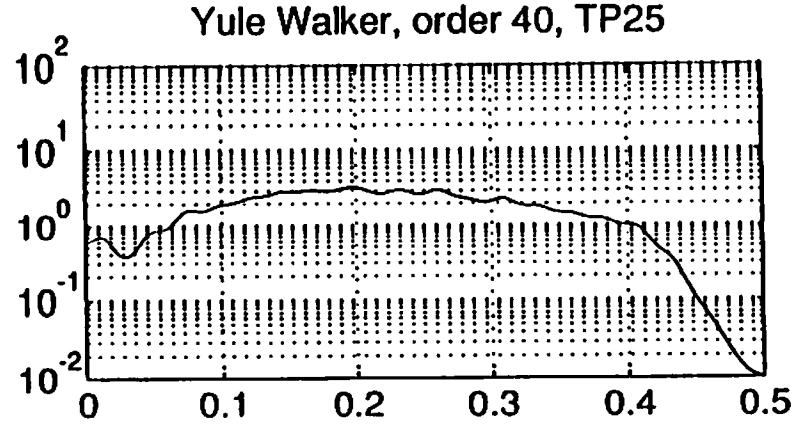


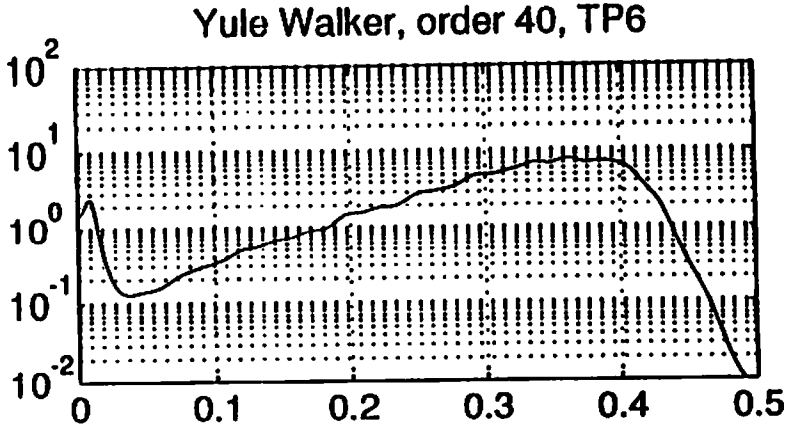


fig. 7.11

using 32768 samples

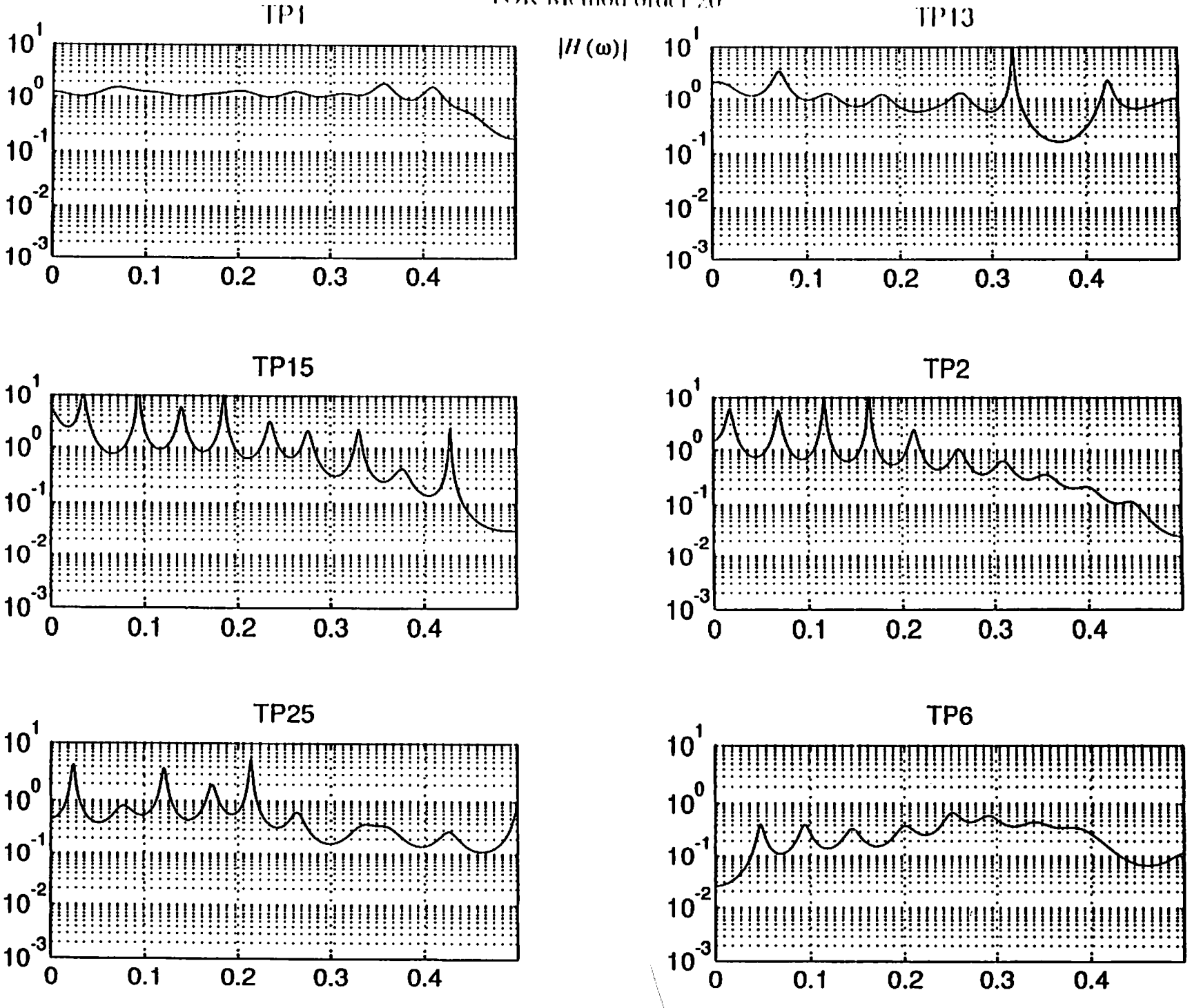


fig. 7.12

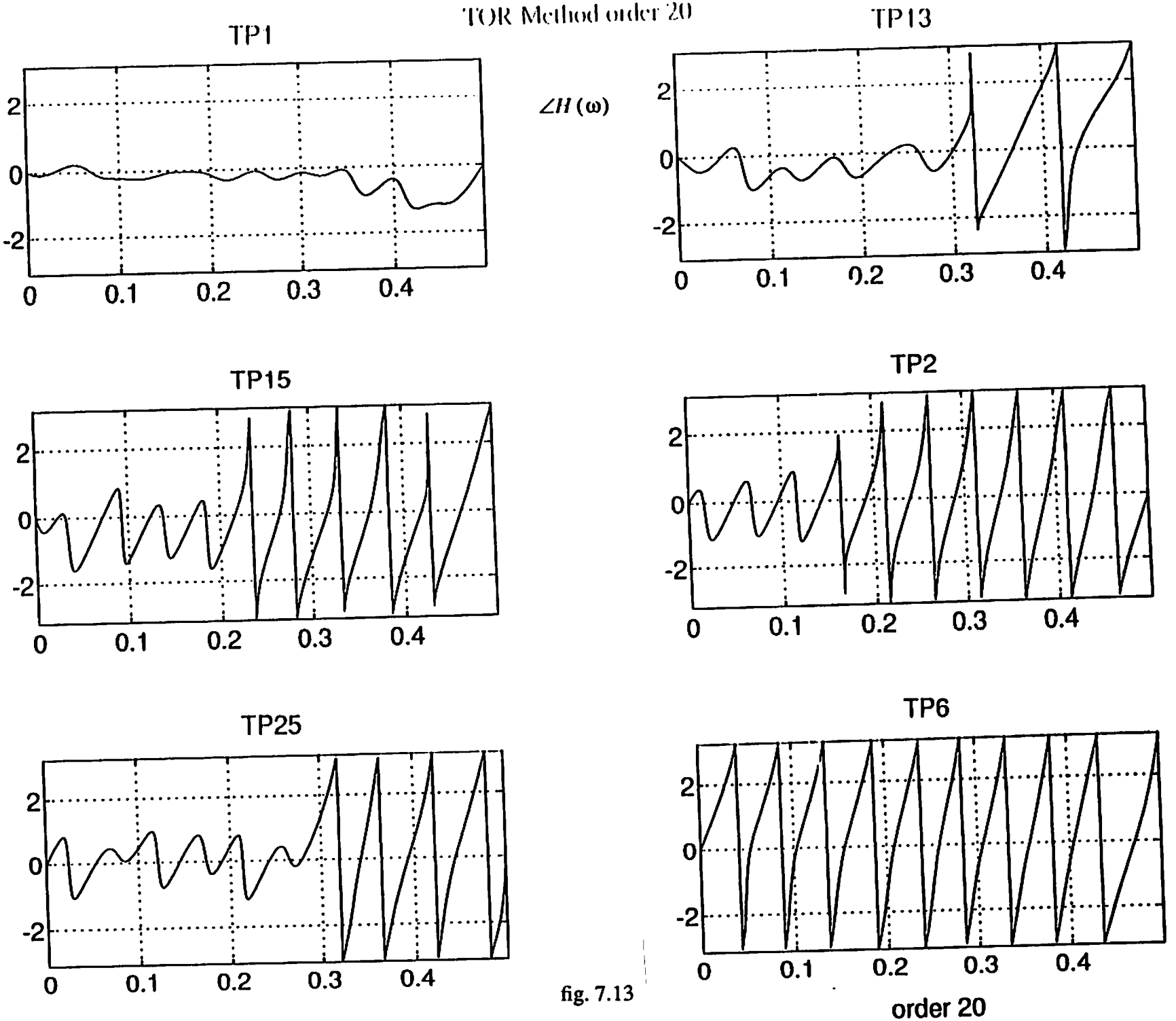
TP1
TP13
$\angle H(\omega)$
TP15
TP2
TP25
TP6
2
0
-2
0
0.1
0.2
0.3
0.4
order 20

fig. 7.13

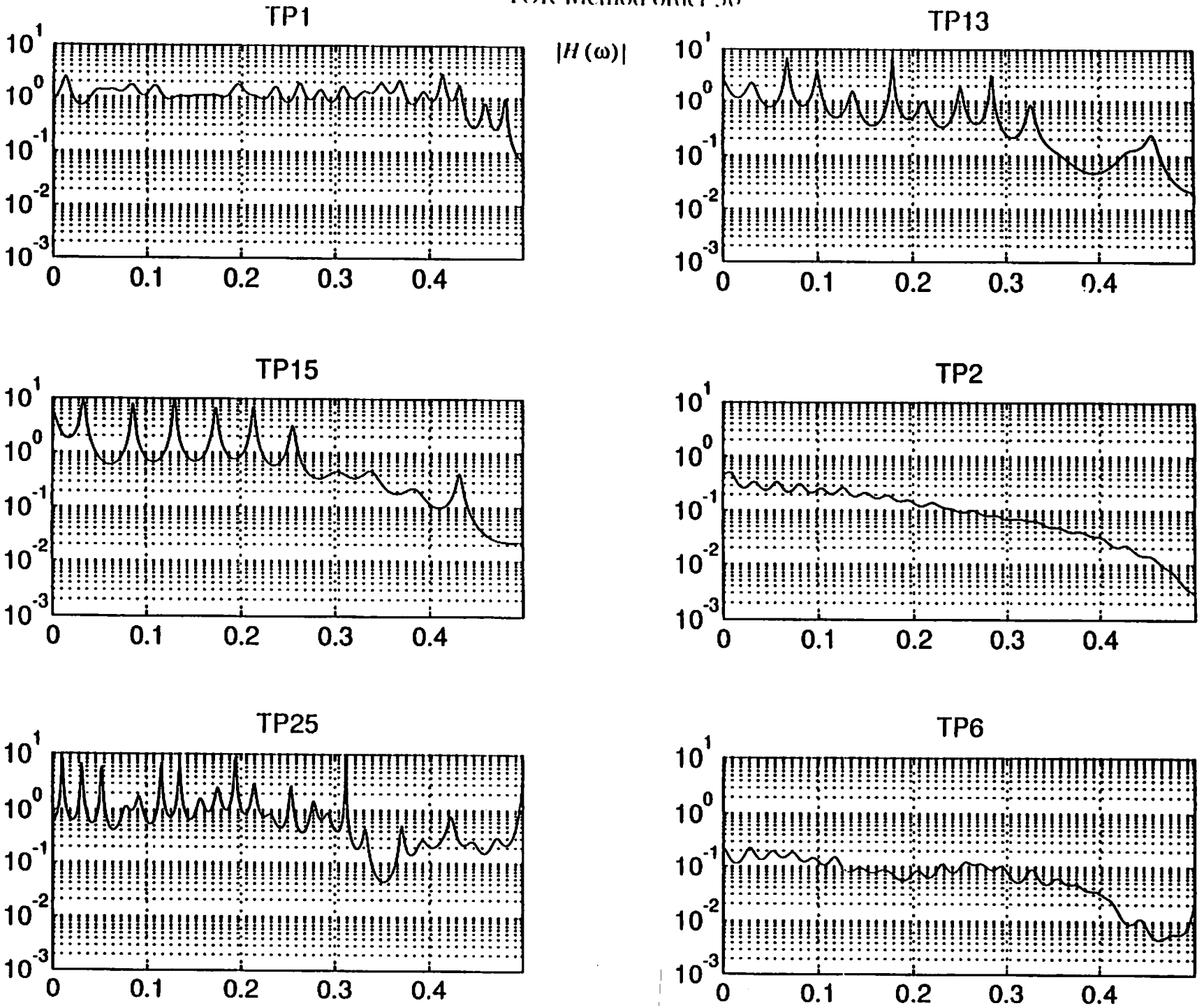
TP1
TP13
TP15
TP2
TP25
TP6
$|H(\omega)|$
$10^{1}$
$10^{0}$
$10^{-1}$
$10^{-2}$
$10^{-3}$
0
0.1
0.2
0.3
0.4

fig. 7.14

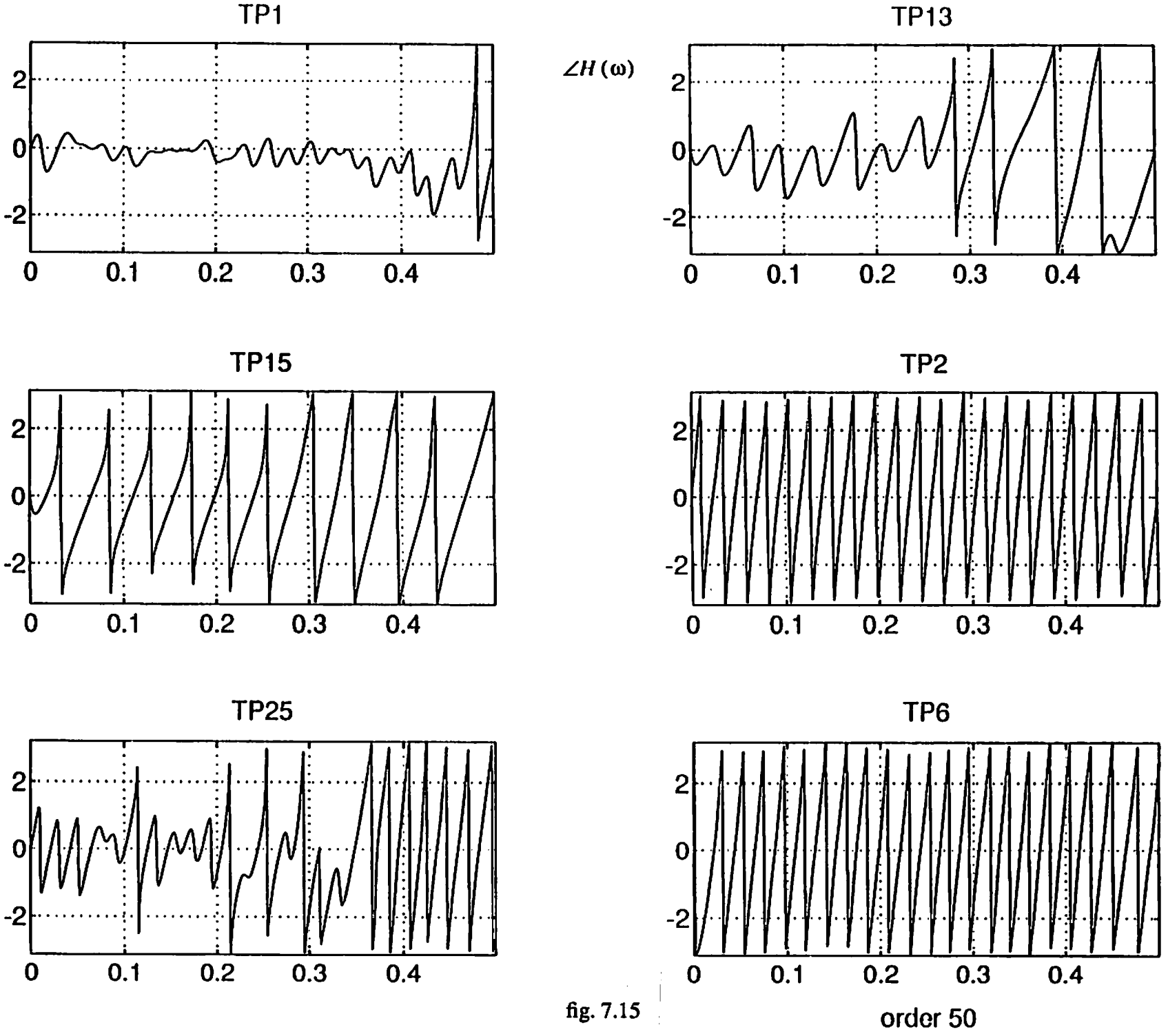
TP1
TP13
$\angle H(\omega)$
TP15
TP2
TP25
TP6
2
0
-2
0
0.1
0.2
0.3
0.4
order 50

fig. 7.15

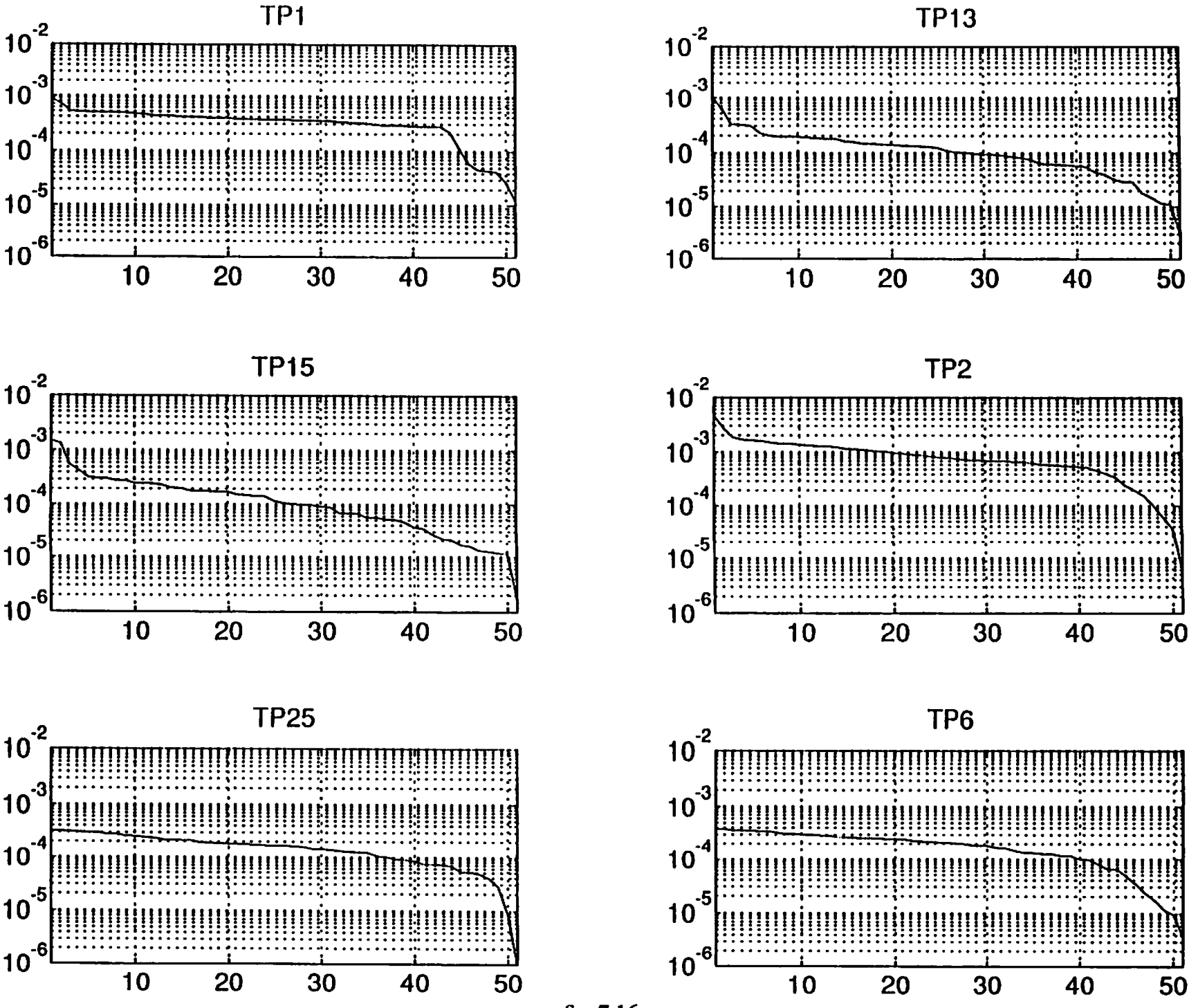


fig. 7.16

SVD of cum. matrix

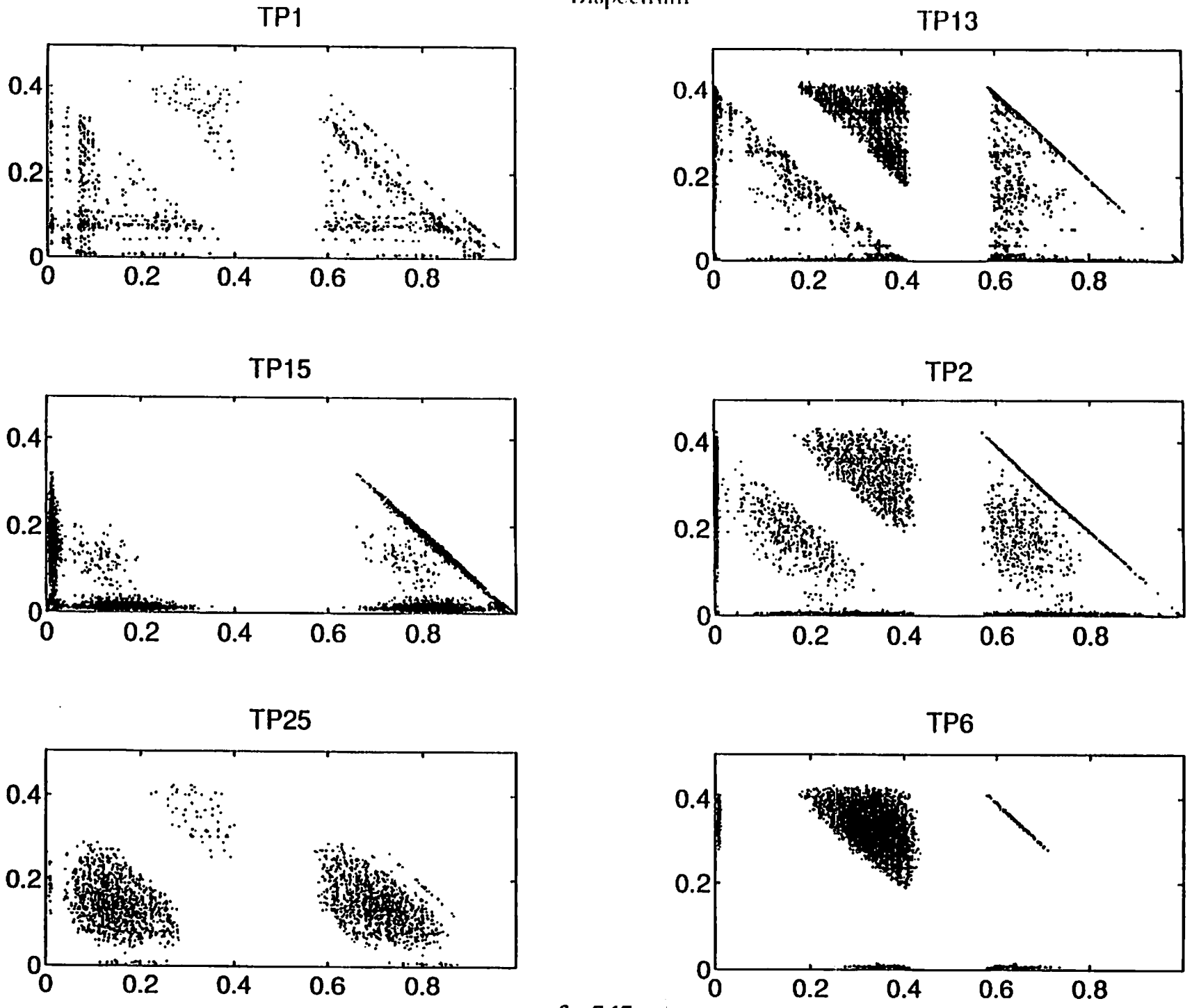


fig. 7.17

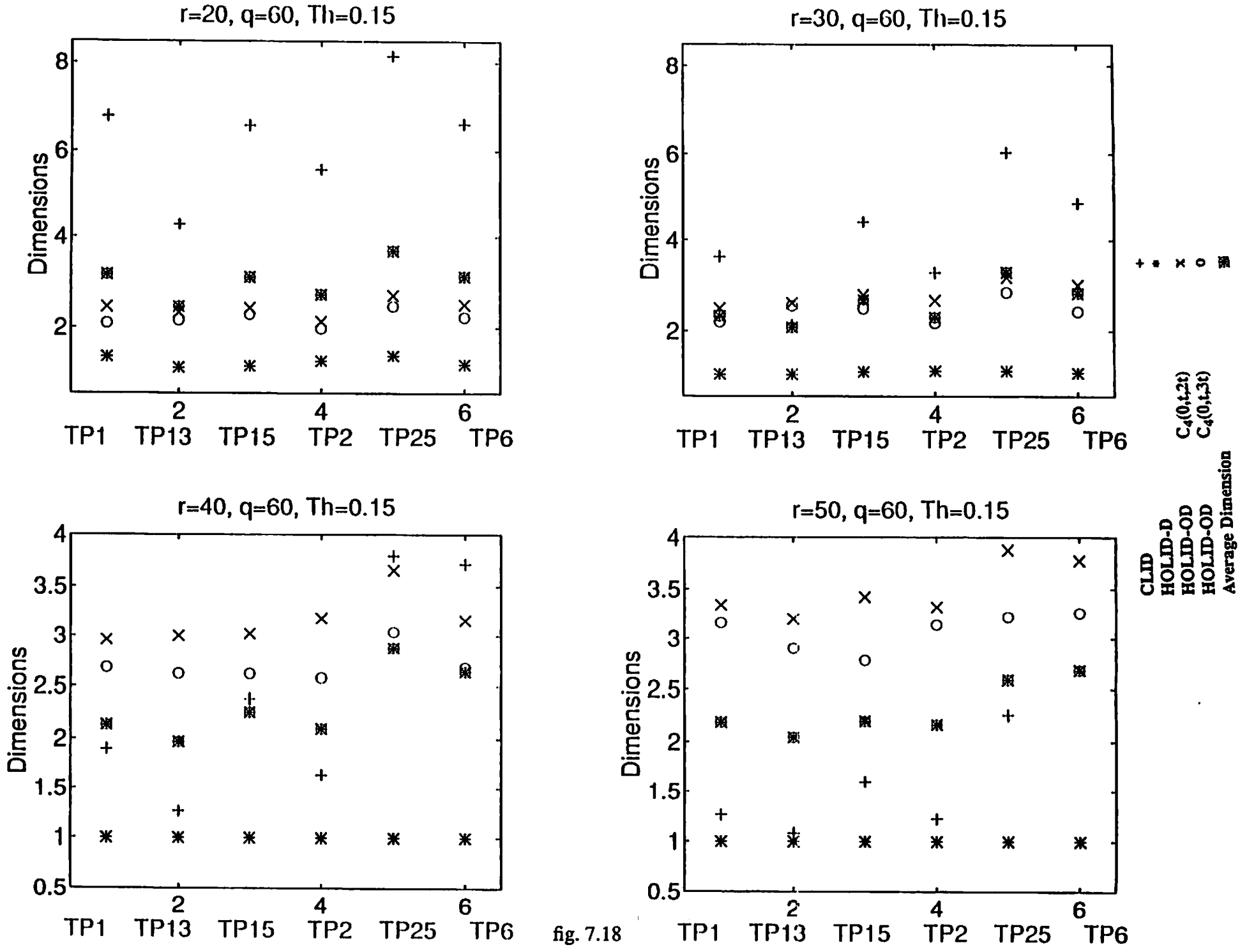
r=20, q=60, Th=0.15
r=30, q=60, Th=0.15
r=40, q=60, Th=0.15
r=50, q=60, Th=0.15
Dimensions
TP1
TP13
TP15
TP2
TP25
TP6
CLID
HOLID-D
HOLID-OD
HOLID-OD
Average Dimension

fig. 7.18

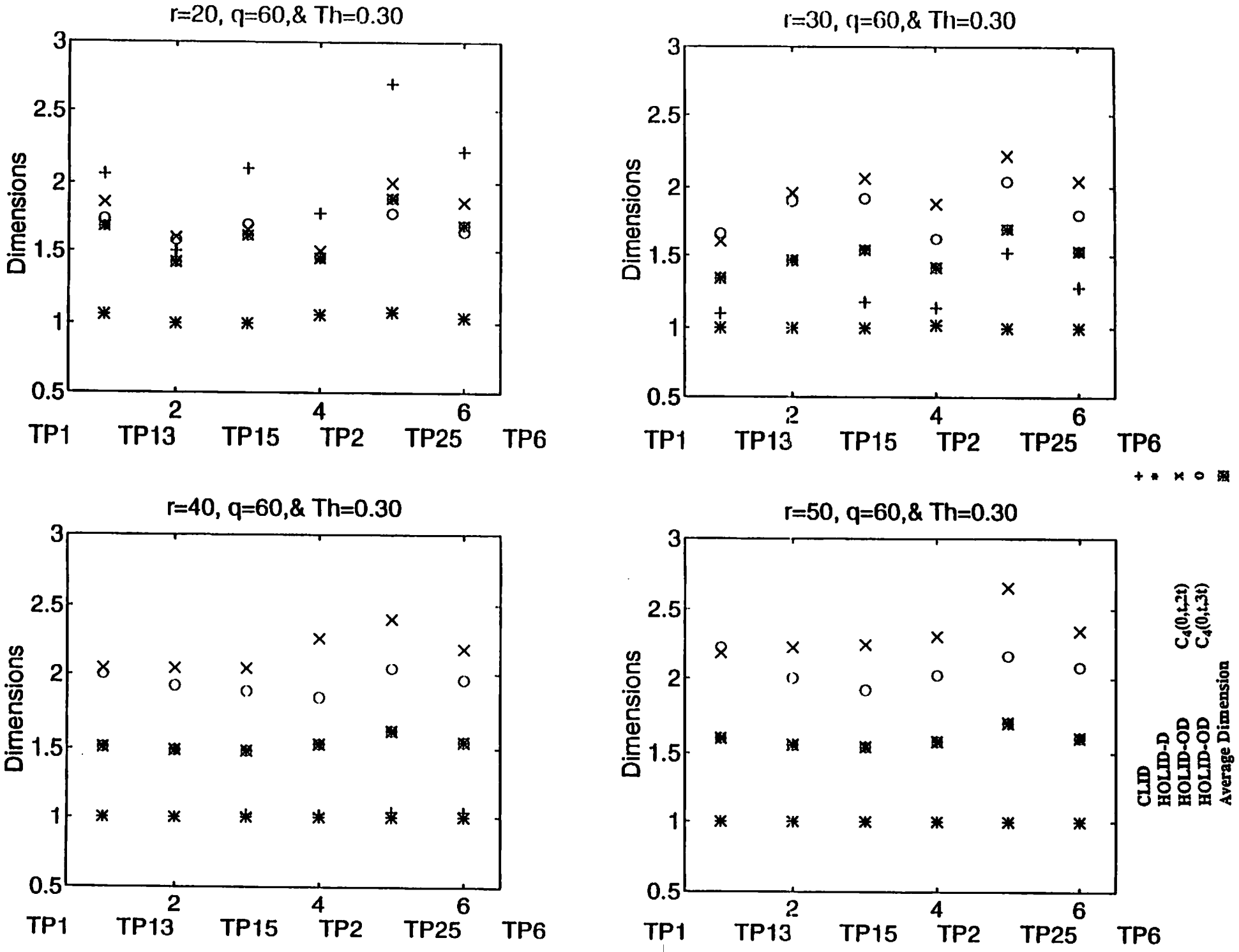
r=20, q=60,& Th=0.30
r=30, q=60,& Th=0.30
r=40, q=60,& Th=0.30
r=50, q=60,& Th=0.30
Dimensions
3
2.5
2
1.5
1
0.5
2
4
6
TP1
TP13
TP15
TP2
TP25
TP6
CLID
HOLID-D
HOLID-OD
HOLID-OD
Average Dimension
$C_4(0,t,2t)$
$C_4(0,t,3t)$

fig. 7.19

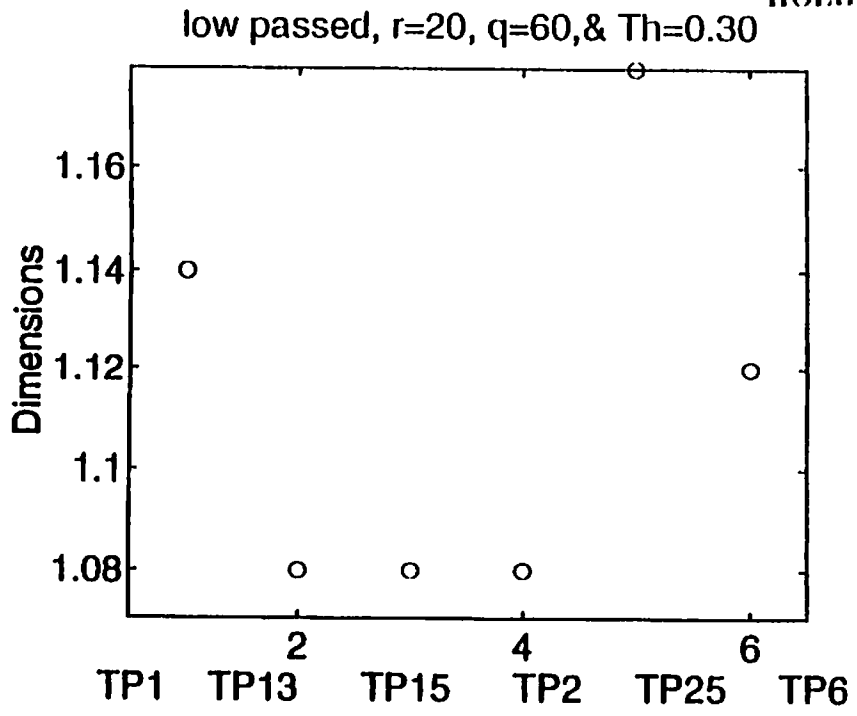
low passed, r=20, q=60,& Th=0.30
Dimensions
1.16
1.14
1.12
1.1
1.08
2
4
6
TP1
TP13
TP15
TP2
TP25
TP6

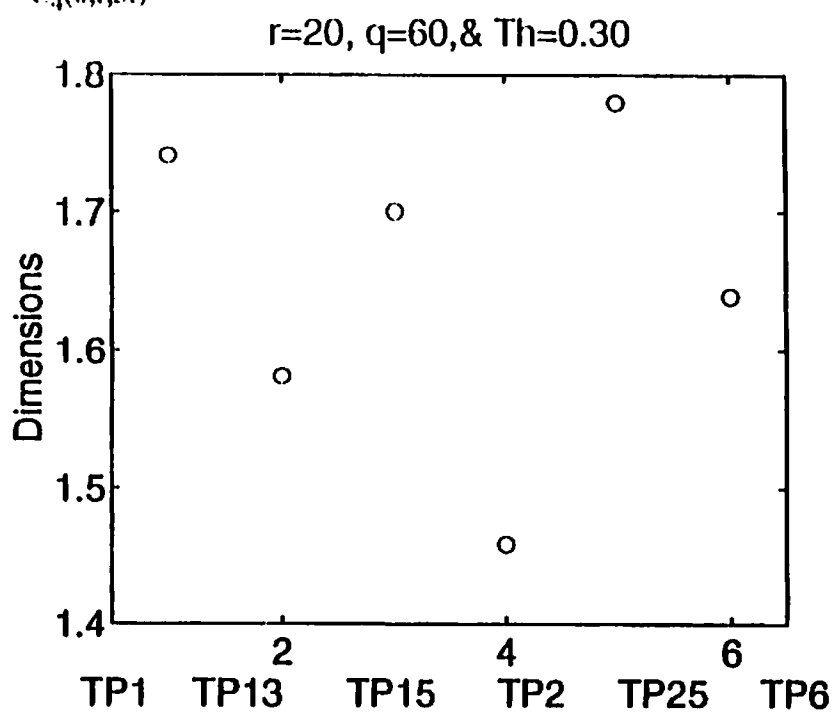
r=20, q=60,& Th=0.30
Dimensions
1.8
1.7
1.6
1.5
1.4
2
4
6
TP1
TP13
TP15
TP2
TP25
TP6

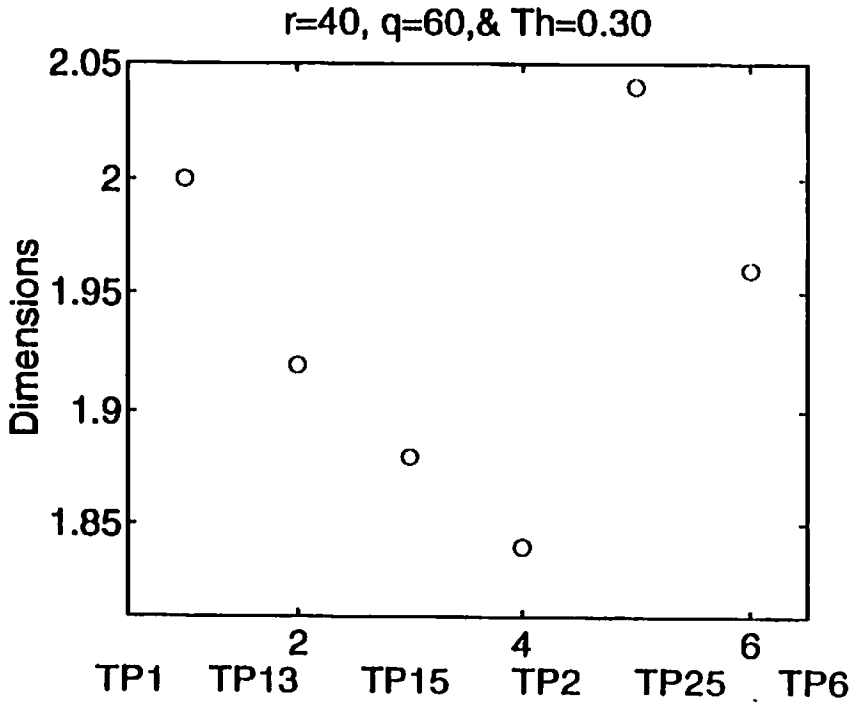
r=40, q=60,& Th=0.30
Dimensions
2.05
2
1.95
1.9
1.85
2
4
6
TP1
TP13
TP15
TP2
TP25
TP6

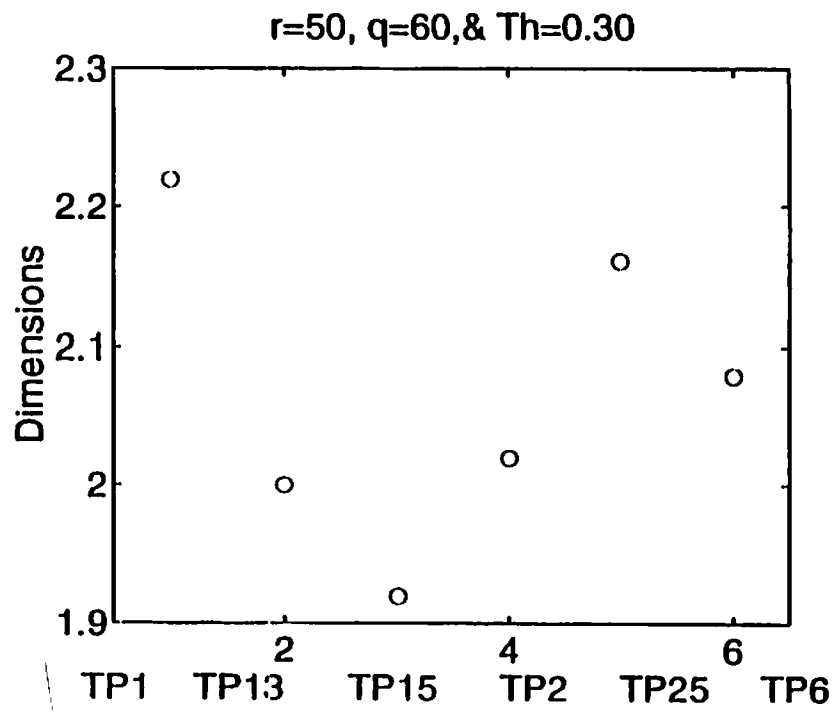
r=50, q=60,& Th=0.30
Dimensions
2.3
2.2
2.1
2
1.9
2
4
6
TP1
TP13
TP15
TP2
TP25
TP6

fig. 7.20

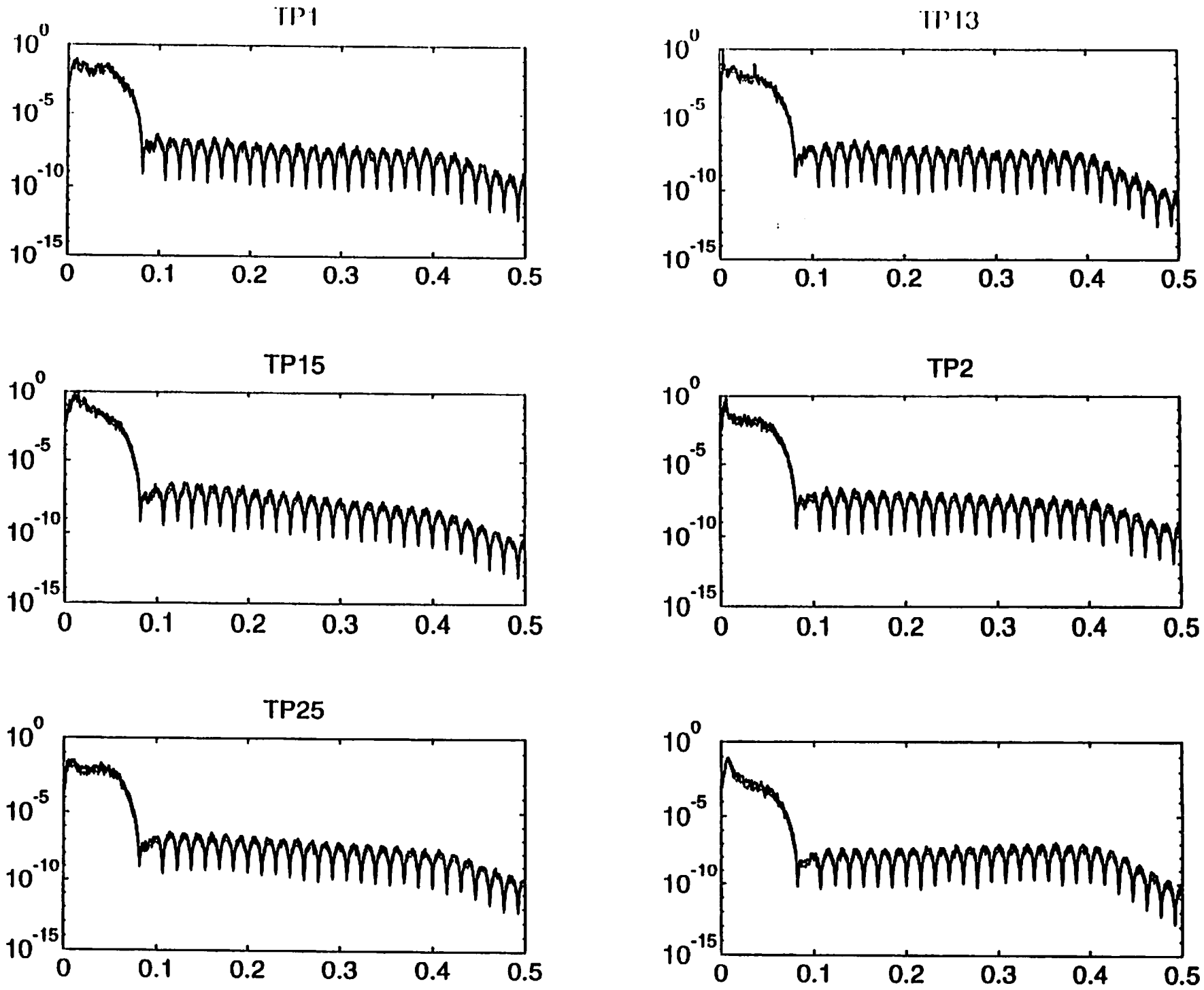


fig. 7.21